Chapter 2

Analysis of Observations

It is a capital mistake to theorize before one has data. Insensibly one begins to twist facts to suit theories, instead of theories to suit facts.

Sherlock Holmes, *A Scandal in Bohemia*

This chapter provides a comprehensive look at available observations of tropical Pacific climate over the past four decades. This analysis is undertaken for several reasons. First, it provides a ground truth for the development and evaluation of the coupled model in the next chapter. Second, it reveals the range of climate, ENSO, and noise variability that are actually observed, which is useful for orienting and interpreting the sensitivity maps of later chapters. Finally, it reveals the level of uncertainty in the observations. The climate differences between observational analyses, between decades, and between different coupled GCMs, underscore the necessity of exploring wide regions of climate parameter space.

Special attention is paid to the wind stress on the ocean surface, for the following reasons. First, the stress is a key variable for both the climatology and ENSO. It largely reflects the gradient of SST, the slope of the thermocline, and the strength of equatorial upwelling; and as one of the noisiest of climate variables, it also provides stochastic forcing to the ENSO system. Second, the wind stress is one of the few variables for which multidecadal records are available. Third, the stress is quite uncertain, so it is useful to compare analyses from different sources. Finally, the detailed analysis of the stress supports the development of the statistical atmosphere model in Chapter 3.

2.1 Preliminaries

2.1.1 Motivation

The wind stress on the ocean surface is of intense interest to the climate community. Modelers depend on realistic wind stresses to test their ocean simulations, and forecasters need them to produce accurate initial conditions for climate predictions. Since the recognition of the El Niño/Southern Oscillation (ENSO) as a major driver of Earth's climate,

greater attention has focused on the tropical Pacific Ocean and several retrospective analyses of wind stresses in that basin have been made available to researchers (McPhaden et al., 1998). Due to the sparsity of historical data, changes in observing systems, and different analysis procedures, these products do not always agree on what reality is like. The purpose of this paper is to compare two of these analyses and paint a clearer picture of the wind stress and its uncertainty.

Oceanographers have long recognized that improvements in ocean models must be supported by improvements in the wind stress forcing (Latif, 1987; McPhaden et al., 1988; Harrison et al., 1989; Landsteiner et al., 1990). Wind stresses drive not only the variations in currents and temperatures associated with the annual cycle and El Niño, but also the noisy fluctuations that confound seasonal forecasts, and the slow changes that alter ENSO behavior on decadal and longer time scales. Coupled climate models indicate that ENSO behavior is sensitive to both equatorial and off-equatorial wind stress responses to sea surface temperature (SST) changes (Neelin, 1990; Kirtman, 1997; An and Wang, 2000; Cassou and Perigaud, 2000). The behavior and predictability of ENSO are also affected by random wind stress noise (Penland and Sardeshmukh, 1995; Kleeman and Moore, 1997; Kirtman and Schopf, 1998; Roulston and Neelin, 2000). Better understanding of the wind stress is therefore essential to improving ENSO modeling and prediction.

2.1.2 Uncertainties in the wind stress

The wind stress on the surface of the ocean is difficult to estimate accurately. Until the recent advent of satellite scatterometry, stress estimates were based on wind velocities estimated from wave heights or measured by anemometers many meters above the surface. Such measurements are prone to both random errors, like incorrect assumptions of anemometer heights, and systematic errors, like incorrect conversions from the Beaufort scale to wind speed (Cardone et al., 1990; Morrissey, 1990). The sparseness of observations in time and space also presents a sampling problem. Binning to reduce random errors and aliasing from small scales must be done carefully, since the stress depends nonlinearly on the wind (Wright and Thompson, 1983), and since filling data gaps can spuriously affect the patterns of spatial variability (Sterl, 2001).

Ultimately the wind velocities or pseudostresses must be converted to surface stresses. This typically involves "bulk" formulae, whose form can depend not only on the wind speed, but also the roughness of the surface, the vertical wind shear, the vertical stability of the atmosphere, the surface currents, and even the drift of the observing platform (Smith, 1988; Cardone et al., 1990; da Silva et al., 1994; Kelly et al., 2001). Such variables can be complicated functions of the observations actually collected at sea.

Researchers interested in decadal climate variability must further contend with the gradual evolution of the observing system, including changes in data density and measurement procedures (Clarke and Lebedev, 1997). One notable change occurred in the late 1970s, as anemometers gradually replaced Beaufort estimates as the preferred method for determining wind velocities. This change is probably responsible for much of the apparent trend in observed wind speeds since 1960 (Ramage, 1987; Peterson and Hasse, 1987; Wright, 1988; Posmentier et al., 1989; Cardone et al., 1990; Michaud and Lin, 1992; Ward,

1992; Ward and Hoskins, 1996; Clarke and Lebedev, 1996), and recently the Comprehensive Ocean-Atmosphere Data Set (COADS) has been modified to account for some of these changes (da Silva et al., 1994). Two other major changes include the deployment of anemometers on the Tropical Atmosphere-Ocean (TAO) buoy array beginning in the 1980s, and the launch of scatterometers on satellites beginning in 1991. While such changes were necessary to improve wind stress estimates, they also force investigators to always consider *nonstationarity of the observing system* as one possible source of decadal changes in the observations.

2.1.3 Additional constraints

Wind stress analyses attempt to reconstruct reality from these sparse observations, biased instruments, and changing observing systems. In the face of such uncertainties, it helps to consider additional constraints besides the wind data.

One approach is to examine the self-consistency of the winds: Zebiak (1990), for example, used a set of linear momentum equations to derive a synthetic pressure field, which was then used to adjust the winds to be consistent with a simple vorticity balance. A second approach is to examine the consistency of the winds with the observed forcing. Ward (1992), Ward and Hoskins (1996), and Clarke and Lebedev (1996, 1997), for example, used observed sea level pressures to assess apparent trends in the trade winds. SST is also a useful constraint, since it largely controls the distribution of atmospheric heating and pressure gradients (Gill, 1980; Lindzen and Nigam, 1987). A third approach is to examine the response of the ocean and use it to infer the wind stress forcing. Kirtman and Schneider (1996), for example, adjusted the FSU wind stress to optimize the SST simulation produced by an ocean GCM. Another indicator of the stress is the thermocline slope, which is nearly in balance with the zonal wind stress at the equator (Neelin et al., 1998). Although decadal changes in the thermocline are hard to discern due to the paucity of subsurface data prior to the 1980s, recent work has taken advantage of ocean GCMs and full four-dimensional assimilation of the observations to infer the wind forcing (Bonekamp et al., 2001).

Present analyses combine several of these approaches to estimate the wind stress. While the analyses use largely the same data sources, they rely on different methods for quality control, filling gaps in the observations, and adjusting the data for consistency with physical expectations. *Objective analyses* attempt to represent the data faithfully, imposing few if any physical constraints between variables. *Subjective analyses* rely on experienced meteorologists to check for consistency among important dynamical variables. *Model analyses* rely on numerical models to enforce physical consistency of the data. Given this range of analysis techniques, it is important to examine results from each to help determine what the "real" wind stress actually is and quantify its uncertainty.

2.1.4 Previous studies

Although the evaluation and intercomparison of tropical wind stresses has a long history, previous studies have generally focused on a single analysis, a short time period, or a single aspect of the stress. The annual cycle of wind stress over the tropical Pacific

was described by McPhaden et al. (1988) and Landsteiner et al. (1990), who examined the 1979–1981 period in analyses from Florida State University (FSU), the University of Hawaii (UH), and the Fleet Numerical Oceanography Center (FNOC). Trenberth et al. (1990) and Yang et al. (1997) studied the annual cycle during the 1980–1986 and 1985–1992 periods, respectively, using data from the European Centre for Medium Range Weather Forecasts (ECMWF). Saji and Goswami (1997) analyzed the annual cycle of wind stress over the 1979–1988 period, using results from 17 atmospheric general circulation models (AGCMs) and data from COADS, ECMWF, and Hellerman and Rosenstein (1983).

Other researchers have investigated the total wind stress or departures from the annual cycle. Reynolds et al. (1989) compared surface winds from ECMWF, the National Meteorological Center (NMC, now NCEP), and the U.K. Meteorological Office (UKMO) between February 1987 and July 1987, and Graham (1994) described decadal changes in the FSU pseudostress between 1971–1976 and 1977–1982. Kleeman et al. (2001) examined the response of wind stress anomalies to SST, comparing results from 27 SST-forced AGCMs against the NCEP and corrected COADS products for 1979–1988. Yang et al. (2001) discussed the seasonal dependence of the wind stress anomalies using the FSU and NCEP products. Latif (1987), Harrison et al. (1989), and Auad et al. (2001) have all found substantial differences between ocean simulations forced by different wind stress products.

Auad et al. (2001) recently examined cross-statistics of the NCEP and merged COADS/FSU stress products over the 1958–1997 period, and found the NCEP product to be weaker along the equator by up to a factor of 2.5 (for the zonal stress) or 3.5 (for the meridional stress). While the two datasets were found to be well-correlated in midlatitudes, they were not well correlated in the poorly-sampled equatorial and east Pacific. Interannual stress variations were found to be coherent between the products but intraseasonal variations were not. Shinoda et al. (1999) likewise found that the NCEP stresses tended to underestimate buoy stresses in low-wind conditions in the west Pacific, and Smith et al. (2001) found that the NCEP product underestimates stresses derived from ship observations under a wide range of conditions.

Recently, studies of the wind stress have been motivated by the need to evaluate new satellite products. Busalacchi et al. (1993) compared the Special Sensor Microwave Imager (SSM/I) satellite stresses with data from ECMWF, NMC, FNOC, FSU, and UH between July 1987 and June 1988, while Meissner et al. (2001) compared the SSM/I wind speeds with those from NCEP and ECMWF between July 1987 and December 1997. The NASA scatterometer (NSCAT) stresses have also been evaluated against the ECMWF analysis over brief periods (Kelly et al., 1999; Yu and Moore, 2000).

Coupled model studies have underscored the importance of the wind stress forcing for ENSO simulation and prediction. Chen et al. (1999) showed that hindcasts of the 1997–1998 El Niño in a simple coupled model were improved when NSCAT stresses were used in place of FSU to generate the ocean initial conditions. Kug et al. (2001) showed similar improvements when the NCEP winds were used instead of FSU during the 1990s. Harrison et al. (2002) constructed several statistical models of the wind stress response to SST anomalies, using 1979–1993 stresses from ECMWF, NCEP, and an AGCM run, and 1988–1996 stresses from a satellite product. They found that coupling these different statistical atmospheres to an ocean GCM produced widely different ENSO simulations,

ranging from damped oscillations to sustained oscillations to a slow drift to a new steady state.

It has thus become clear that available wind stress analyses exhibit large differences over the tropical Pacific, and that these differences are large enough to affect simulation of the tropical climatology and ENSO. The analyses also cover different regions and time periods, complicating their use in ocean hindcasts. Current efforts aim to quantify the uncertainties in the analyses (Smith et al., 2001; Taylor, 2001), and integrate the best aspects of different analyses into a single merged solution (Putman et al., 2000). Until such products come into widespread use, researchers who study climate change or need to force ocean models with realistic winds must choose from among several different analyses. The present study should assist in that choice.

2.1.5 Goals of this study

Since the tropical Pacific wind stress plays such a pivotal role in global climate, and since the differences between wind stress products are clearly important for ENSO modeling and forecasting, we here present a more comprehensive look at this field in two widely-used analyses. We also examine the relationship between the wind stress and SST, since this relationship matters a great deal to ENSO, and since simulating it accurately remains a challenge in current atmospheric models (Saji and Goswami, 1997; Kleeman et al., 2001). The primary objectives of this study are to (1) document the similarities and differences between the analyses, (2) show how the analyzed wind stresses have changed over the past four decades, and (3) determine whether these wind stress changes are consistent with SST changes. The results should be of great interest to ENSO researchers, modelers and forecasters.

2.2 Data

The present study focuses on two different analyses of the monthly-mean wind stress. The first, referred to as FSU, is the subjectively-analyzed Florida State University pseudostress (Legler and O'Brien, 1988; Stricherz et al., 1997), available from the Center for Ocean-Atmospheric Prediction Studies. The FSU data are routinely used for climate studies, forcing ocean models, and generating initial conditions for ENSO forecasts (Chen et al., 1995; Dewitte and Perigaud, 1996, ; see also Introduction). The present study uses only the FSU research-quality product, which as of this writing is available from 1961–1999. The FSU pseudostress $\|\mathbf{u}_a\|\mathbf{u}_a$ is converted to wind stress $\boldsymbol{\tau}$ using the bulk formula

$$\boldsymbol{\tau} = \rho_a c_d \|\mathbf{u}_a\|\mathbf{u}_a \tag{2.1}$$

where $\rho_a = 1.2$ kg m^{-3} is the surface air density and $c_d = 1.3 \times 10^{-3}$ is a nondimensional drag coefficient.

The second stress product, referred to as NCEP, is the model-based NCEP/NCAR reanalysis (Kalnay et al., 1996), available from the LDEO/IRI Climate Data Library. The reanalysis is available from 1949 to the present, and has been used for climate studies (see Introduction), atmospheric model comparisons (Kleeman et al., 2001), ocean hindcasts

(Behringer et al., 1998), and operational ENSO forecasts (Ji et al., 1998). It should be noted that the reanalysis classifies the zonal stress as a type "B" variable (observed but also strongly influenced by the model), and the meridional stress a type "C" variable (derived solely from the model and forced to remain close to the atmosphere simulation).

An objective analysis of the Comprehensive Ocean-Atmosphere Data Set (COADS, da Silva et al., 1994) has also been examined but for brevity will not be presented here. These data have been used in studies of decadal climate change (Kleeman et al., 1999) due to their availability over a long period (1945-1993) and their relative freedom from analysis biases. Results for this product were very similar to those for FSU, in large part because FSU is based heavily on COADS after 1966. An overview of ENSO-related aspects of COADS can be found in Harrison and Larkin (1998).

The monthly-mean SSTs used in this study are from the reconstruction of Smith et al. (1996), available from the NOAA-CIRES Climate Diagnostics Center. These SSTs have been used for climate studies (An and Wang, 2000), because they span the entire 1950-1999 period using a uniform statistical scheme. This helps to reduce spurious discontinuities resulting from changes in analysis procedures and data density.

The monthly-mean data are averaged onto identical grids with 5.625° longitude by 2° latitude spacing over the tropical Pacific region (129.375°E–84.375°W, 20°S–20°N). Land points are excluded from the analysis, but the data are not detrended. A 12-month climatology is computed for each dataset over the 1961–1999 period (468 months), and subtracted from the total fields to give monthly-mean anomalies. A similar decomposition is performed separately for the 1961–1979 period (228 months) and the 1980–1999 period (240 months). We refer to the wind stress anomalies as $\boldsymbol{\tau}'$, the zonal and meridional components as τ_x' and τ_y', and the SST anomalies as SSTA.

The split into pre-1980/post-1980 timeseries serves two purposes. First, it provides an estimate of slow trends in the wind stress. Second, it separates the earlier period of relatively sparse observations from the latter period of intensive observations and more modern methods. Changes in the analyzed stresses between these two periods will therefore be a product of two confounding effects: changes in the physical system and changes in the observing/analysis system. By comparing two different analyses, it is possible to separate these two effects somewhat. Differences between the analyses afford an estimate of the level of uncertainty in the wind stress, which can then be used to assess similar changes in the analyses.

2.3 Climatology

2.3.1 Annual mean

The annual-mean climatologies of the wind stress and SST are shown in Fig. 2.1. The zonal component of the mean stress, $\overline{\tau}_x$ (Fig. 2.1a), is easterly everywhere except in the far eastern and western equatorial Pacific. These easterlies are important for producing mean equatorial upwelling and a shoaling of the thermocline in the eastern Pacific, both of which are key to understanding the annual cycle and ENSO. The trade winds have a slanted saddle shape: they peak in the central basin 12°–15° poleward of the equator, weaken towards the equator, and then weaken further towards the equatorial coasts. Compared to FSU,

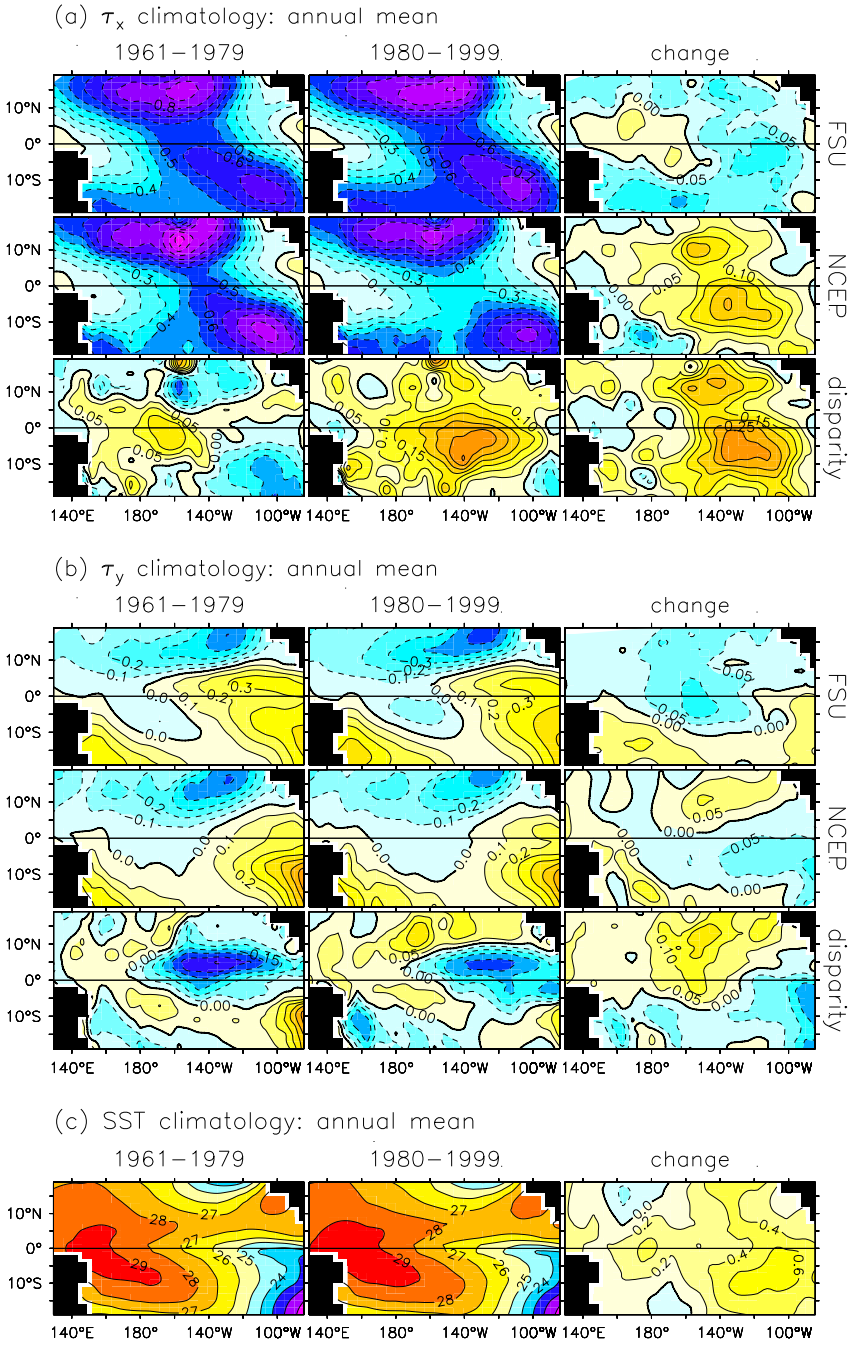

Figure 2.1: Annual-mean climatology of (a) zonal wind stress (dPa), (b) meridional wind stress (dPa), and (c) SST (°C). Fields are shown for 1961–1979 (first column) and 1980–1999 (second column). The change from the former period to the latter is also shown (third column). Rows correspond to the FSU analysis (first row), the NCEP analysis (second row) and their difference (NCEP minus FSU, third row).

NCEP has a more pronounced saddle shape, with weaker easterlies at the equator. Between 1961–1979 and 1980–1999, both products show a weakening of the easterlies around the equatorial dateline and a strengthening in the southwest. However, while FSU shows a strengthening of the trade winds east of 160°W, NCEP shows a weakening in this region. In other words, while FSU suggests the climatological trade winds strengthened and shifted eastward, NCEP suggests they weakened and shifted westward.

Fig. 2.1b shows $\overline{\tau}_y$, the meridional component of the mean stress. Southerly winds cross the equator in the east Pacific and meet opposing northerlies in the Intertropical Convergence Zone (ITCZ) along 5°N–12°N. These southerlies are important for generating mean upwelling south of the equator, which increases the coupling of the surface and subsurface in the eastern Pacific. In the central basin, weak northerlies cross the equator and meet opposing southerlies in the South Pacific Convergence Zone (SPCZ) along 5°S–17°S. Compared to FSU, NCEP shows stronger southerlies in the southeast, but weaker southerlies crossing the equator in the central and eastern Pacific. Between 1961–1979 and 1980–1999, both FSU and NCEP suggest an increase of the southerlies in the southwest. Along the southeast coast, however, FSU indicates that the southerlies along the southeast coast strengthened while NCEP suggests they weakened. The decadal changes in $\overline{\tau}_y$ also contrast strongly between the analyses in the northern tropical Pacific.

The mean curl of the wind stress (not shown) is associated primarily with meridional gradients of $\overline{\tau}_x$. The curl is positive north of the equator and in the western equatorial and southeastern tropical Pacific; the curl is negative in the eastern equatorial and southwestern tropical Pacific. The mean cyclonic curl on both sides of the equator is important because it produces divergence of ocean surface currents away from the equatorial zone, raising the mean thermocline. The NCEP curl is more strongly cyclonic than in FSU. Between 1961–1979 and 1980–1999, both products show a strengthening of the cyclonic curl in the southwest, but other decadal changes are not well correlated between the products.

The mean wind divergence (not shown) is thought to be important for controlling the sensitivity of atmospheric heating to SST perturbations (Zebiak and Cane, 1987; Tziperman et al., 1997; Galanti and Tziperman, 2000; Wang, 2000a). The ITCZ and SPCZ slant equatorward toward the west and meet in the equatorial western Pacific. FSU shows much stronger convergence zones than NCEP, and stronger divergence in the equatorial eastern Pacific. Between 1961–1979 and 1980–1999, both FSU and NCEP show increased convergence in the western equatorial Pacific, but other changes are not consistent. For example, FSU shows a weakening of the mean divergence in the equatorial eastern Pacific, while NCEP shows a strengthening of this divergence.

The tropical climatology is a result of strong air-sea feedbacks (Dijkstra and Neelin, 1995; Philander et al., 1996) so that any discussion of the winds must include consideration of the SST. The SST climatology (Fig. 2.1c) consists of a vast warm pool of > 28°C water in the west, a smaller warm pool south of Mexico, a warm band of > 27°C water north of the equator that connects the warm pools, and a cold tongue of water that extends up the coast of South America and westward along the equator. The edges of these features delineate regions of strong horizontal SST gradients which give rise to the wind stress climatology: the northward SST gradient along the equator in the east induces the cross-equatorial southerlies, and the westward SST gradient in the central Pacific enhances the equatorial

easterly trade winds. The SST data suggest that between 1961–1979 and 1980–1999, there was a warming and eastward expansion of the western warm pool, a widening of the warm band, and an eastward shrinking of the cold tongue. The maximum warming occurs in the cold tongue region, indicating a weakening of the zonal SST contrast across the basin.

To the extent that the trade winds are driven by hydrostatically-induced pressure gradients associated with SST gradients (Lindzen and Nigam, 1987), the warming in the east Pacific would seem to suggest a general weakening of the easterlies, consistent with NCEP. However, in the west Pacific the latent heating of the middle troposphere is an important driver of the winds (Wang and Li, 1993). Because the supply of moisture available for latent heating depends nonlinearly on SST (through the Clausius-Clapeyron relation and horizontal moisture convergence), the winds are arguably more sensitive to SST changes in the west Pacific (where the SST is warm) than in the east (where the SST is cold). If this is the case, then the warming and eastward expansion of the warm pool would seem consistent with the strengthening and eastward shift of the trade winds seen in FSU.

Thus it is not immediately clear which of the products has the more realistic annual-mean stress, and clearly simple qualitative arguments are not sufficient to resolve this question. It is hoped that Fig. 2.1 will motivate further evaluation of the stress climatologies using comprehensive atmosphere and ocean models.

2.3.2 Annual cycle

Standard deviations associated with the climatological annual cycle are shown in Fig. 2.2. As described by McPhaden et al. (1988), there are strong variations of $\overline{\tau}_x$ and $\overline{\tau}_y$ associated with the western Pacific monsoons and the seasonal movements of the ITCZ. Most of the variability occurs in broad bands along 10°N and 10°S, west of the dateline and in the ITCZ. The annual cycle of the wind stress is substantially weaker along the equator and in the southeast Pacific. Variability of the climatological wind stress curl and divergence are concentrated at the northern and southern edges of the ITCZ. FSU generally shows much stronger seasonal variability of $\overline{\tau}_y$ and divergence due to the stronger ITCZ in that product, although NCEP does show stronger variability north of 10°N and in the far southeastern basin.

Between 1961–1979 and 1980–1999, both FSU and NCEP show increased monsoonal $\overline{\tau}_x$ variability in the southwest and decreased variability in the southeast. However, while FSU shows strengthening annual variations of the central Pacific easterlies and east Pacific cross-equatorial southerlies, NCEP indicates the opposite. For the stress curl there is little agreement between the analyses, with FSU showing increased variability near the equator and NCEP showing a broad decrease in variability across the east Pacific. For the stress divergence, both analyses show the increased seasonal variability in the central equatorial Pacific, and decreased variability of the ITCZ, but elsewhere the changes are not consistent between FSU and NCEP. Interestingly, the SST annual cycle hardly changes between 1961–1979 and 1980–1999.

Time/longitude plots of the annual cycles of $\overline{\tau}_x$ and SST at the equator are shown in Fig. 2.3. The annual cycle of SST is strongest in the eastern Pacific (near 100°W) where temperatures are warmest in March and coolest in September. The annual signal propagates westward, with SST changes in the east leading those at the dateline by 3–4

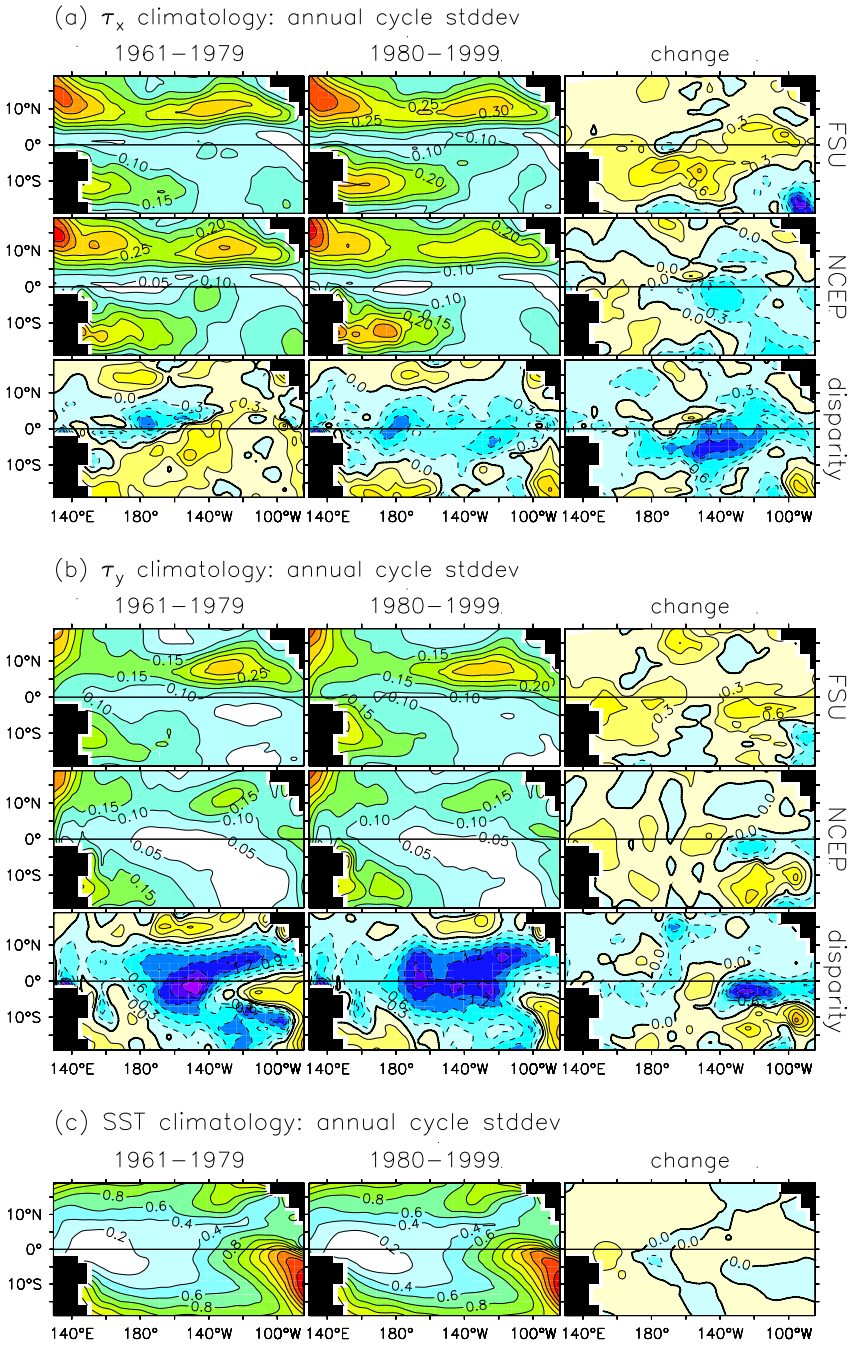

Figure 2.2: Standard deviations associated with the climatological annual cycle of (a) zonal wind stress (dPa), (b) meridional wind stress (dPa), and (c) SST (°C). Standard deviations are shown for 1961–1979 (first column) and 1980–1999 (second column). The base 2 logarithm of the ratio of the latter period over the former is also shown (third column). Rows correspond to the FSU analysis (first row), the NCEP analysis (second row), and the base 2 logarithm of their ratio (NCEP over FSU, third row).

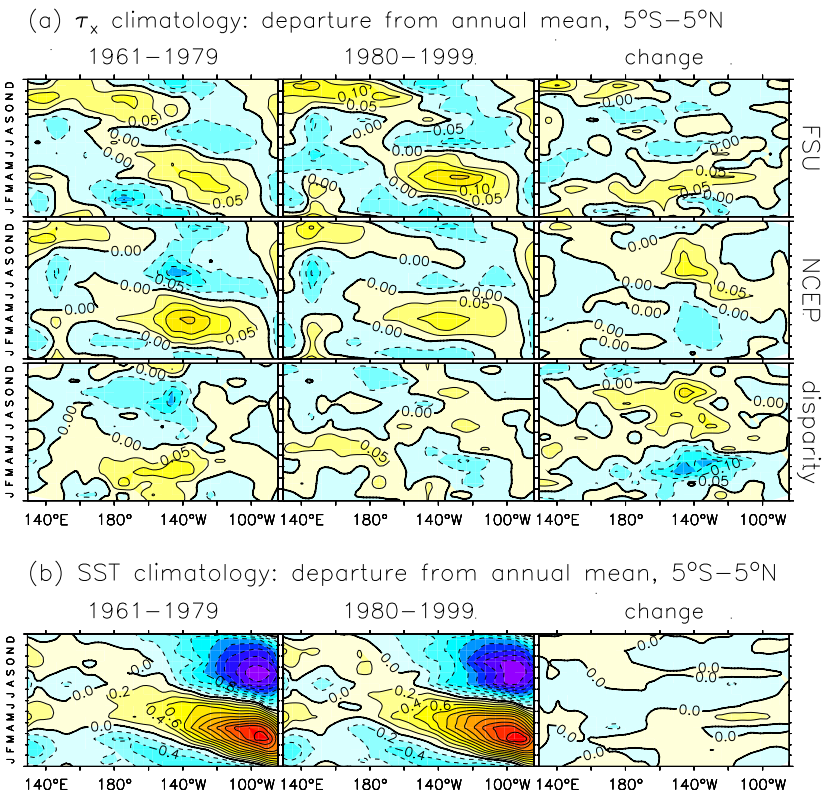

Figure 2.3: Climatological annual cycle of deviations from the annual mean, averaged over the equatorial band from 5°S to 5°N, for (a) zonal wind stress and (b) SST.

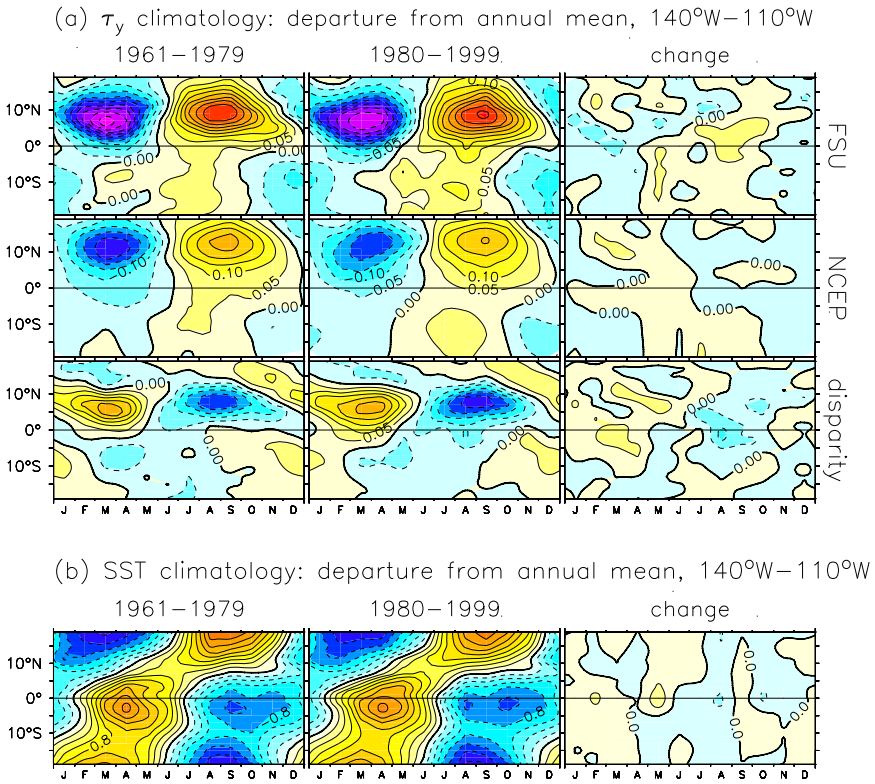

Figure 2.4: Climatological annual cycle of deviations from the annual mean, averaged over the eastern Pacific from 140°W to 110°W, for (a) meridional wind stress and (b) SST.

months. The zonal gradient of SST at the equator is weakest in boreal spring and strongest in boreal autumn, consistent with the strong annual cycle of $\overline{\tau}_x$ near 140°W that shows weakened easterlies in boreal spring. In the west Pacific there is a prominent semiannual cycle, with westerlies and warm SST in May and November, and easterlies and cool SST in February and August.

In both wind stress products between 1961–1979 and 1980–1999, the semiannual signal in the west is largely replaced by an annual signal, with westerlies in boreal winter and easterlies in boreal summer. In the eastern equatorial Pacific the annual signal strengthens in FSU but weakens in NCEP. The SST data indicate a slight decadal warming in May in the east, and a slightly *stronger* semiannual cycle in the west, but otherwise there is very little change in the annual cycle of SST at the equator.

Latitude/time plots of the annual cycles of $\overline{\tau}_y$ and SST in the eastern Pacific are shown in Fig. 2.4. Away from the equator, the SST cycle is in quadrature with the solar cycle: maximum temperatures appear in autumn following the summer season of strong solar heating, and minimum temperatures appear in spring following the winter season of weak heating. SST changes at the equator closely track those of the south Pacific, with the strongest variability occurring just south of the equator in the heart of the equatorial cold tongue. The seasonal changes of $\overline{\tau}_y$ are strongest north of the equator at the southern edge of the ITCZ. The annual cycle of $\overline{\tau}_y$ in both hemispheres is nearly in phase with the SST in the north; In contrast with the large north/south phase difference in SST, the $\overline{\tau}_y$ changes in the north lag those in the south by only 1–2 months. The northward SST gradient, cross-equatorial southerly winds, and equatorial wind divergence are all strongest in boreal summer/autumn and weakest in boreal winter/spring.

The annual cycle of $\overline{\tau}_y$ is much stronger in FSU than in NCEP, especially north of the equator associated with the stronger ITCZ in FSU. Neither the SST nor the $\overline{\tau}_y$ data indicates much change in the eastern annual cycle between 1961–1979 and 1980–1999.

2.3.3 Summary

Clearly the FSU and NCEP wind stress climatologies differ substantially. Perhaps most important for ENSO modeling are the differences in (1) equatorial $\overline{\tau}_x$ (weaker in NCEP), which controls the strength of equatorial upwelling, the zonal slope of the thermocline, and is linked with evaporative cooling of the sea surface; (2) mean off-equatorial cyclonic stress curl (stronger in NCEP), which affects the zonal-mean depth of the equatorial thermocline; (3) cross-equatorial southerlies in the eastern Pacific (weaker in NCEP), which produce upwelling just south of the equator; and (4) mean equatorial convergence (weaker and less seasonally-variable in NCEP), which in simple models controls the sensitivity of the atmosphere to heating anomalies.

The analyses also disagree regarding the nature of the mean wind stress changes between 1961–1979 and 1980–1999, with the equatorial $\overline{\tau}_x$ weakening in NCEP but strengthening and shifting eastward in FSU. Because of the subtlety of the decadal SST changes, it is difficult to say which product is the more correct regarding decadal changes in the annual mean stress. The large (and conflicting) changes in the annual cycle of $\overline{\tau}_x$ are also puzzling, given the lack of substantial changes in the annual cycle of SST between 1961–1979 and 1980–1999. Either the stress changes are not real, or they are caused by something other

than variations in SST; perhaps nonlinearity (associated with the mean warming observed in Fig. 2.1c), or changes in extratropical heating or land heating. Assuming the SST reconstruction is accurate, these puzzles could presumably be solved using an atmospheric GCM to evaluate the wind stress response to observed SST changes, or an ocean GCM to check the ocean response to the wind stress changes (e.g. Graham, 1994).

2.4 Anomaly patterns

2.4.1 Interannual variability

Fig. 2.5 shows standard deviations of the wind stress anomalies and SSTAs at periods greater than one year. The interannual variability of τ_x' (Fig. 2.5a) is concentrated in the central equatorial Pacific. These τ_x' variations are important for several reasons: they induce changes in the zonal slope of the thermocline, they generate zonal currents which advect water at the edge of the warm pool, and they alter the strength of equatorial upwelling, all of affect equatorial SST. Except for NCEP 1961–1979, the center of action for τ_x' appears just east of the dateline, near the 28°C isotherm at the edge of the warm pool. In this region the standard deviation of interannual τ_x' is roughly twice that of the annual cycle, and is half the strength of the annual mean. There is little τ_x' variability near the coasts.

FSU and NCEP differ substantially in their representation of interannual τ_x'. For 1961–1979, the interannual variations of τ_x' in NCEP are shifted almost 40° east of FSU. For 1980–1999, the interannual variability in NCEP shifts westward to within 10° of FSU, but then its standard deviation is only ∼60% of FSU. Between these two periods, FSU shows an increase in interannual τ_x' variance almost everywhere except north of 5°N in the central basin. NCEP, on the other hand, shows a strong *decrease* of variance across the entire eastern half of the basin.

Interannual variability of τ_y' (Fig. 2.5b) is focused near the climatological edges of the ITCZ and SPCZ. In FSU the standard deviation of τ_y' is double that in NCEP, presumably due to the stronger convergence zones in FSU. Between 1961–1979 and 1980–1999, the interannual variability of τ_y' increases along the equator in both datasets, especially FSU. The weakening of interannual τ_y' in NCEP between 5°S–10°S is not as evident in FSU.

Interannual anomalies of wind stress curl (not shown) are focused in the central Pacific around 5°N and 10°S, at the northern and southern edges of the τ_x' variability. Variations in wind stress curl are thought to be important because they generate off-equatorial Rossby waves, which discharge warm surface waters away from the equator and terminate El Niño. The interannual curl variability is stronger in FSU than NCEP. FSU also shows a broad decadal increase in interannual curl variability across the basin, while NCEP shows *decreased* curl variability in the east. These changes are consistent with the changes in interannual τ_x' variability noted above.

Interannual anomalies of wind stress divergence (not shown) are most active in the central Pacific, especially in FSU associated with the strong ITCZ in that product. Changes in wind divergence are important because they are associated with convective changes over the eastern Pacific, which alter the surface heat balance and may affect the sensitivity of the atmosphere to SST. The analyses show relatively weak interannual variability of the

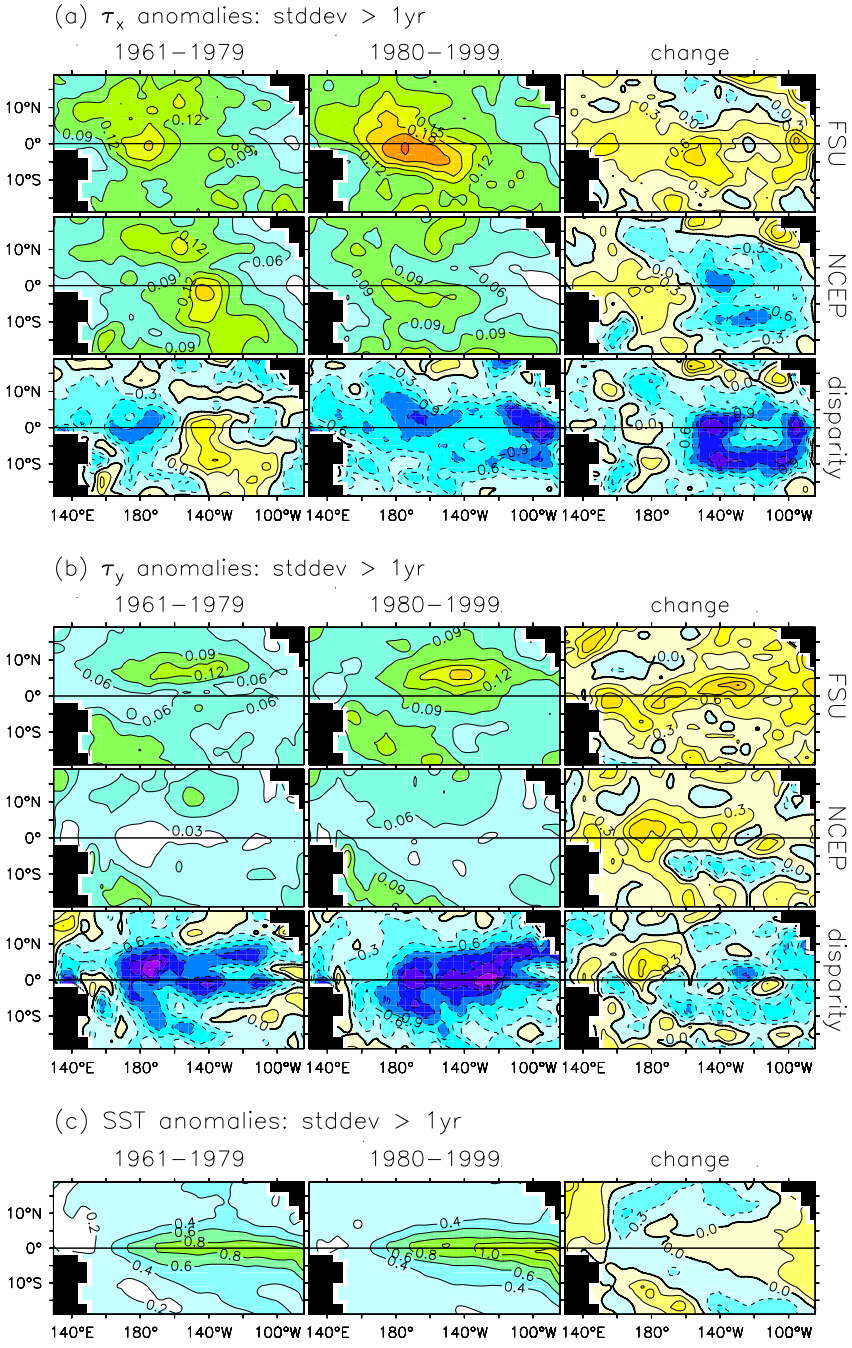

Figure 2.5: As in Fig. 2.2, but for the standard deviation of anomalies at periods greater than one year. The monthly-mean anomalies are filtered by two applications of a 6-month running mean, which gives a spectral half-power point at 12.4 months.

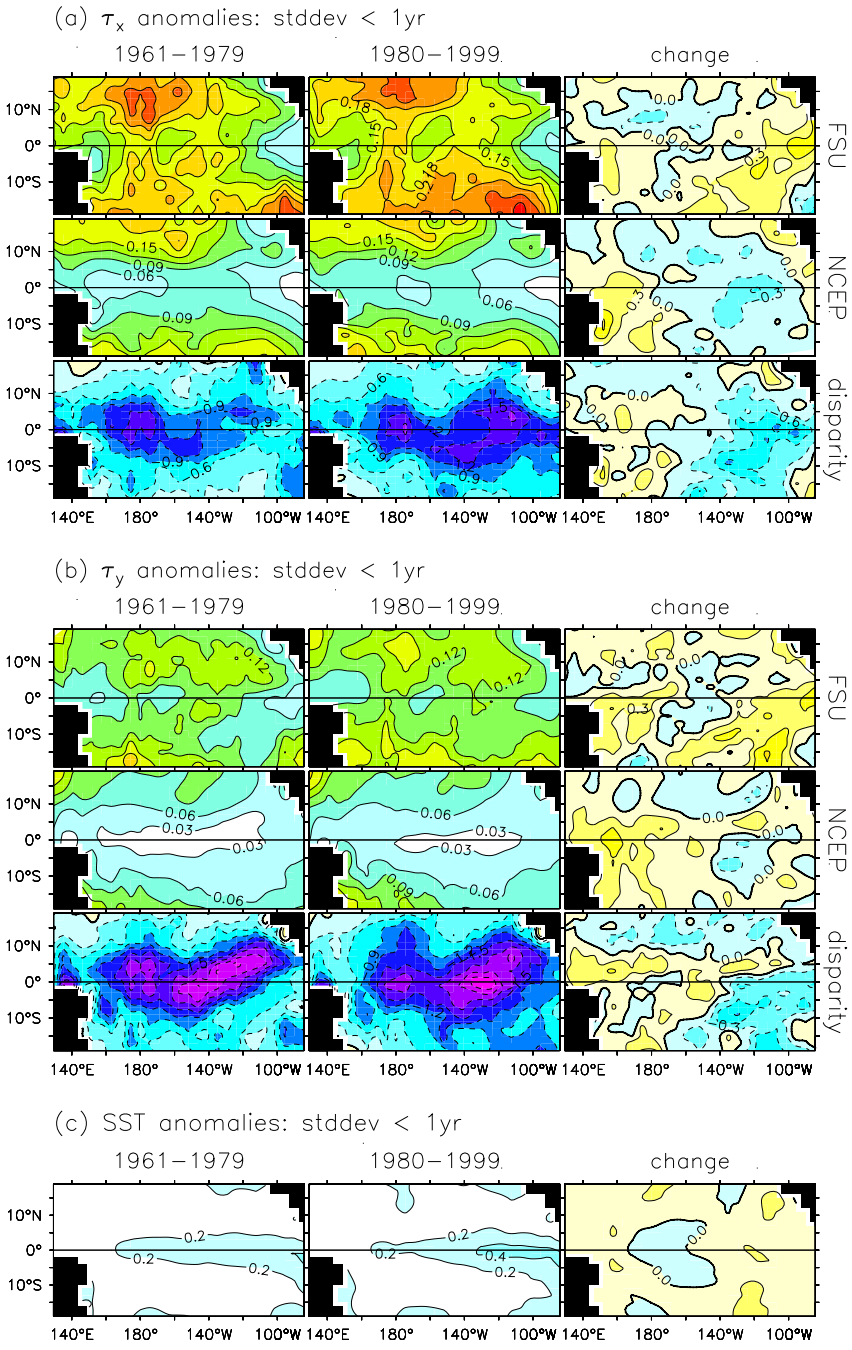

Figure 2.6: As in Fig. 2.5, but for variability at periods less than one year. This is the variability remaining when the interannual component of Fig. 2.5 is subtracted from the monthly-mean anomalies.

divergence in the far western equatorial Pacific. The interannual divergence variability is stronger in FSU than NCEP. Between 1961–1979 and 1980–1999, FSU shows an increase in interannual divergence variability in the east and a decrease in the west, while NCEP shows an *increase* in the west and a decrease off-equator in the central and eastern tropical Pacific.

For SSTA (Fig. 2.5c), interannual variability is concentrated near the equator in the eastern Pacific along the cold tongue. There is very little interannual SSTA variability in the western equatorial Pacific and away from the equator. Between 1961–1979 and 1980–1999, the SSTA variability increases in the far eastern and western Pacific, and decreases at 160°E and in the off-equatorial central basin.

2.4.2 Subannual variability

Fig. 2.6 shows standard deviations of the monthly anomalies at periods less than one year. This short-period variability is thought to play a role in triggering and amplifying ENSO events. The subannual τ_x' is weak near the coasts (especially in the east), but away from the equator the subannual component is even stronger than the interannual component. At the equator, FSU indicates the subannual τ_x' is as strong as the interannual τ_x', while NCEP shows a much weaker subannual component. Between 1961–1979 and 1980–1999, both FSU and NCEP show a strengthening of subannual τ_x' variance in the west Pacific and a weakening in the central Pacific around 5°N–10°N. In FSU, however, the subannual variance in the east Pacific increases, while in NCEP it decreases.

For τ_y', the subannual variability is generally comparable to the interannual variability. Apart from a broad minimum near the equator, there is little agreement between FSU and NCEP regarding the structure of the subannual τ_y' variance. In particular, FSU has much stronger equatorial variance than NCEP. Between 1961-1979 and 1980-1999, both products show increased variance in the west. FSU, however, shows a much stronger increase in the east than NCEP.

The subannual curl and divergence anomalies (not shown) are also much stronger in FSU than NCEP, especially near the equator. For both the subannual curl and the subannual divergence, FSU shows increased variability in the far eastern and western equatorial Pacific. The decrease in variability over the central Pacific is focused farther west in FSU than in NCEP.

For SSTA, subannual variability is focused in the cold tongue region much like the interannual variability. The subannual component, however, is much weaker than the interannual component in this region. The lack of subannual variance is partly due to the SST reconstruction procedure (Smith et al., 1996) and the regridding done in this study; in particular, tropical instability waves, which are active in the cold tongue region with a period of 20–40 days and wavelengths of 10°–20° longitude, are practically eliminated by the temporal and spatial averaging. Yet examination of high-resolution SSTs from the weekly optimal interpolation of Reynolds and Smith (1994) indicates that the subannual variance is generally less than 30% as strong as the interannual variance in the cold tongue region during 1981–2001. Thus much of the strong subannual variability in the wind stress is probably not caused by subannual SSTA. Between 1961–1979 and 1980–1999, the subannual variance of SSTA increases slightly in the east Pacific and decreases slightly

near 160°W, but such small changes could easily be due to the increase in the density of observations between the two periods.

2.4.3 Response to SST anomalies

Model studies have shown that ENSO behavior is quite sensitive to subtle changes in the wind stress response to SST anomalies (Neelin, 1990; Kirtman, 1997; An and Wang, 2000; Cassou and Perigaud, 2000), so it is important to understand the observed response. The stress response is a function of season (Yang et al., 2001) and also differs between warm events and cold events (Kang and Kug, 2002). For purposes of comparison, however, it is useful and illuminating to simply show the annually-averaged, linear response to SSTA.

Regressions of the wind stress anomalies and SST anomalies onto SSTA averaged over the NINO3 region (150°W–90°W, 5°S–5°N) are presented in Fig. 2.7. These regressions are performed without regard to the seasons or total SST, and in this sense represent the "average" response to a warm anomaly in the eastern Pacific.

Both stress products indicate equatorial westerlies and off-equatorial easterlies in the west/central basin, weak easterlies near the eastern boundary, northerlies spanning the northern tropical Pacific, and southerlies across the southwest and equatorial southeast Pacific. There is cyclonic stress curl on both sides of the equator in the central Pacific, convergence along the equator, and divergence in the off-equatorial eastern Pacific. The stress response is not entirely symmetric about the equator. The meridional center of the τ_x' response lies a degree or two south of the equator, and the center of the northern cyclone ($\sim 5°$N) is closer to the equator than the center of the southern cyclone ($\sim 10°$S). Between 1961–1979 and 1980–1999, the FSU and NCEP τ_x' responses to NINO3 SSTA (Fig. 2.7a) undergo a few similar changes; at the equator, these include stronger westerly anomalies near the dateline, stronger easterly anomalies near the western boundary, and weaker easterly anomalies near the eastern boundary.

Yet there are also many striking differences between the analyses. For 1961–1979, the equatorial westerlies (and associated off-equatorial cyclonic curl) in the two products have similar amplitudes, but in FSU the response is centered near 175°W while in NCEP it is focused near 145°W with only a weak tail extending past the dateline. For 1980–1999, the two products are in better agreement regarding the position of the westerly peak near 165°W, but the NCEP response is less than 60% as strong as that in FSU during this period. Thus while FSU indicates that the westerly response to NINO3 SSTA strengthened and spread eastward between 1961–1979 and 1980–1999, NCEP suggests just the opposite.

The meridional stress response (Fig. 2.7b) also differs substantially between FSU and NCEP. Although the NCEP response looks somewhat more similar to FSU during 1980–1999 than during 1961–1979, for both periods NCEP shows weaker southerly stress anomalies in the SPCZ region and equatorial eastern Pacific, and much weaker meridional convergence anomalies than FSU in the vicinity of the ITCZ. Between 1961–1979 and 1980–1999, FSU suggests a change toward a more northerly wind stress response at the equator near 140°W, while NCEP shows a smaller change occurring 20°–30° farther west.

Fig. 2.7c shows how SST anomalies are related to the NINO3 index. Between 1961–1979 and 1980–1999, the SSTA pattern shifted eastward by 5°–10°, and the strength of anomalies in the equatorial eastern Pacific increased. To the extent that the wind stress is

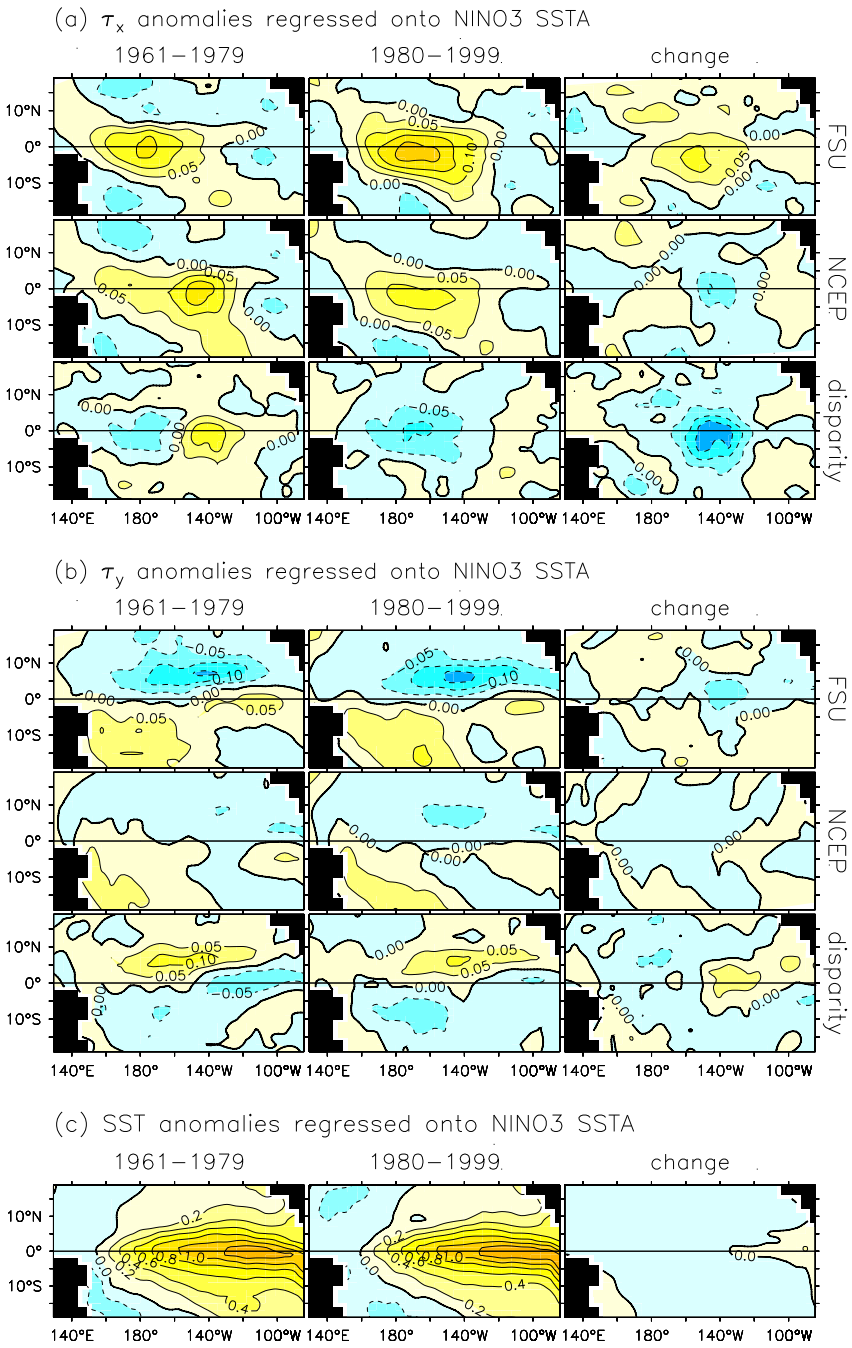

Figure 2.7: As in Fig. 2.1, but for regressions of anomalies onto NINO3-average SST anomalies. Units as in Fig. 2.1 but divided by °C.

linearly determined by SST gradients, these changes appear consistent with the eastward shift and strengthening of the stress response found in FSU. More complicated dynamics would be required to explain the westward shift and weakening of the stress response found in NCEP.

One must ask whether the very small decadal changes in the SSTA pattern can account for the rather large changes in *either* of the wind stress analyses, if indeed the stress changes are real. It is known that the atmospheric heating which drives the winds is a nonlinear function of the total SST and wind convergence (Kleeman, 1991; Wang and Li, 1993; Battisti et al., 1999; Cassou and Perigaud, 2000). Therefore it is possible that changes in mean SST and wind convergence between 1961–1979 and 1980–1999 (Fig. 2.1c) could play as large a role in modifying the stress response as the small changes in the structure of the SST anomalies. Again, qualitative arguments are not adequate to resolve this question; quantitative investigations with comprehensive atmospheric models will be required.

2.4.4 Point correlations

Point correlations of the FSU and NCEP wind stress anomalies are shown in Fig. 2.8. In general, the correlation between the two products is higher for τ_x' than τ_y', higher in the west than the east, higher for interannual periods than subannual periods, and higher for 1980–1999 than 1961–1979. Exceptions include the very low, even negative, interannual correlation in the eastern Pacific during 1961–1979, and the slight decrease in off-equatorial subannual correlation between 1961–1979 and 1980–1999.

It is no surprise that the correlations are lowest in the eastern Pacific, where the ENSO signal is weakest (Figs. 2.5–2.6), and during the earlier period, where the observations are sparse (McPhaden et al., 1998). Sampling problems are also probably to blame for the low correlations (below 0.5) of subannual anomalies near the equator. In contrast, the interannual τ_x' correlations in the western-central equatorial Pacific during 1980–1999 are quite high, approaching 0.95. Clearly recent improvements in the observing system, such as the deployment of the TAO array, have led to better agreement between the wind stress analyses.

2.5 Anomaly timeseries

Interdecadal averages and their differences tell only part of the story of the wind stress. In this section we focus on key regions for interannual τ_x' and SSTA and take a closer look at the temporal character of the data. As shown in Fig. 2.5, the center of action for τ_x' is the NINO4 region in the western equatorial Pacific (160°E–150°W, 5°S–5°N), while that for SSTA is the NINO3 region in the eastern equatorial Pacific (150°W–90°W, 5°S–5°N)

2.5.1 The timeseries

Standardized timeseries of NINO4 τ_x' and NINO3 SSTA are shown in panels (a) of Figs. 2.9–2.11. The standard deviation scale σ and lag-1-month autocorrelation ϕ_1 of the timeseries are indicated above each plot. Note that the standard deviation of FSU is nearly twice that of NCEP. The NINO3 SST anomalies ($\phi_1 = 0.91$) are more persistent in time

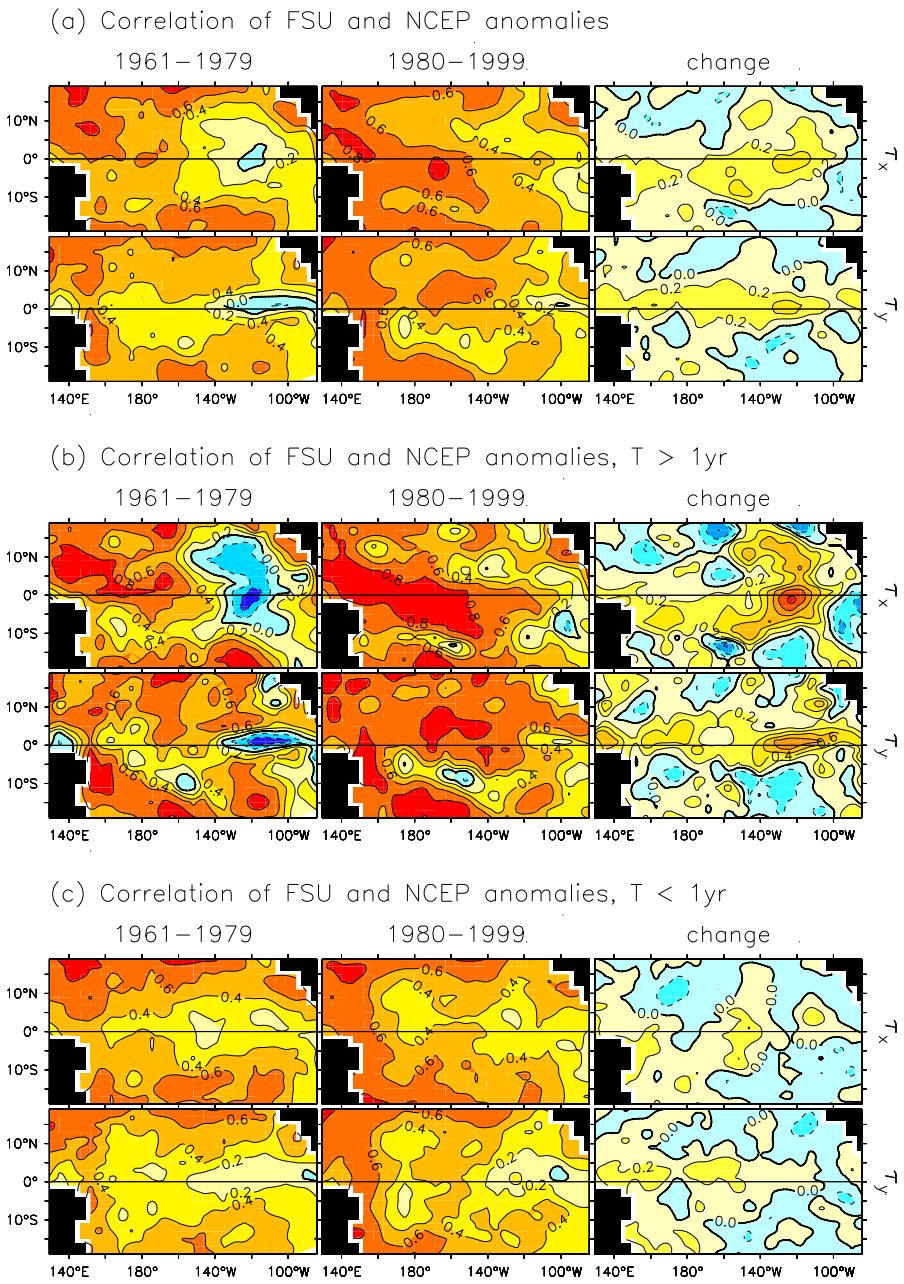

Figure 2.8: Point correlation of FSU and NCEP wind stress anomalies, for (a) the full anomalies, (b) anomalies filtered to retain only periods greater than 1 yr, and (c) anomalies filtered to retain only periods less than 1 yr. Fields are shown for 1961–1979 (first column) and 1980–1999 (second column). The change from the former period to the latter is also shown (third column). Rows correspond to the zonal stress anomalies (first row) and the meridional stress anomalies (second row).

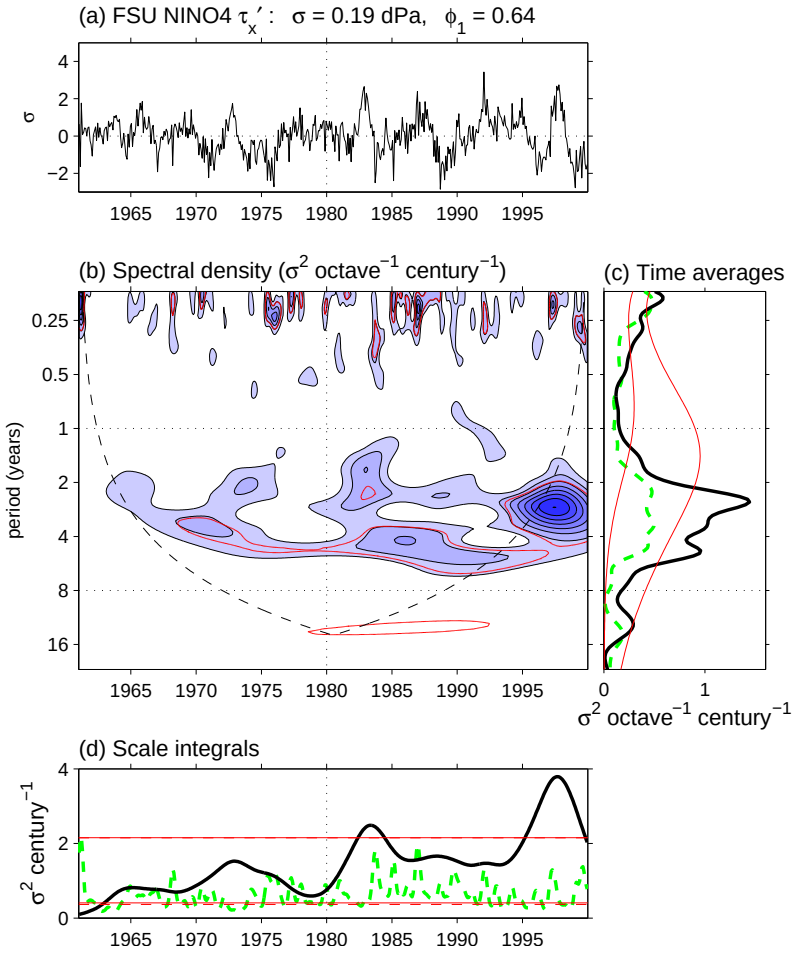

Figure 2.9: (a) Timeseries of standardized monthly anomalies for the FSU zonal wind stress averaged over the NINO4 region (160°E–150°W, 5°S–5°N). Anomalies are with respect to the 1961–1999 climatology. The standard deviation σ and lag-1 autocorrelation ϕ_1 are indicated at the top of the plot. (b) Spectral density of the timeseries, obtained by convolution with a wavenumber-6 Morlet wavelet. The base contour and contour interval are 0.5 σ^2 octave^{-1} century^{-1}. The dashed line ("cone of influence") represents twice the e-folding time for the wavelet response to a spike in the timeseries; below this line the spectral density is underestimated due to edge effects. Thick contour encloses the 95th percentile for red noise realizations with the same σ and ϕ_1 as the timeseries. (c) Time-averaged spectra for 1961–1979 (thick dashed) and 1980–1999 (thick solid). Thin lines bracket the central 90% of wavelet spectra calculated from 20-year realizations of the red noise. (d) Running variance in the 0–1 year spectral band (thick dashed) and the 1–8 year band (thick solid). Thin lines bracket the central 90% of running variances calculated from red noise.

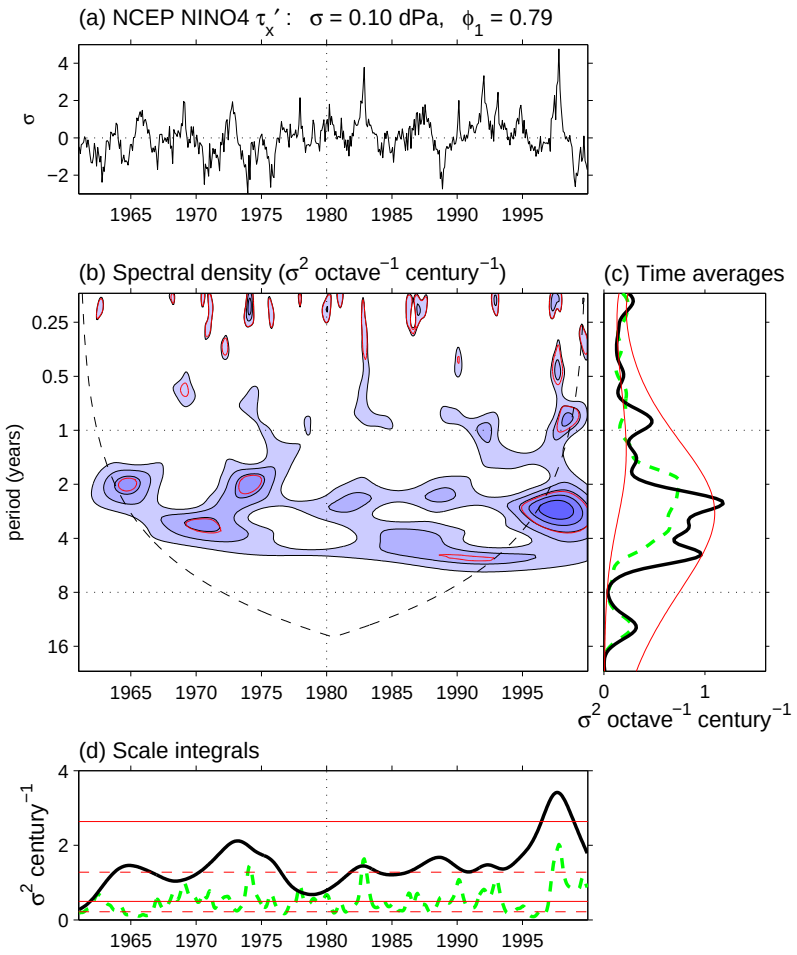

Figure 2.10: As in Fig. 2.9 but for the NCEP zonal wind stress anomalies.

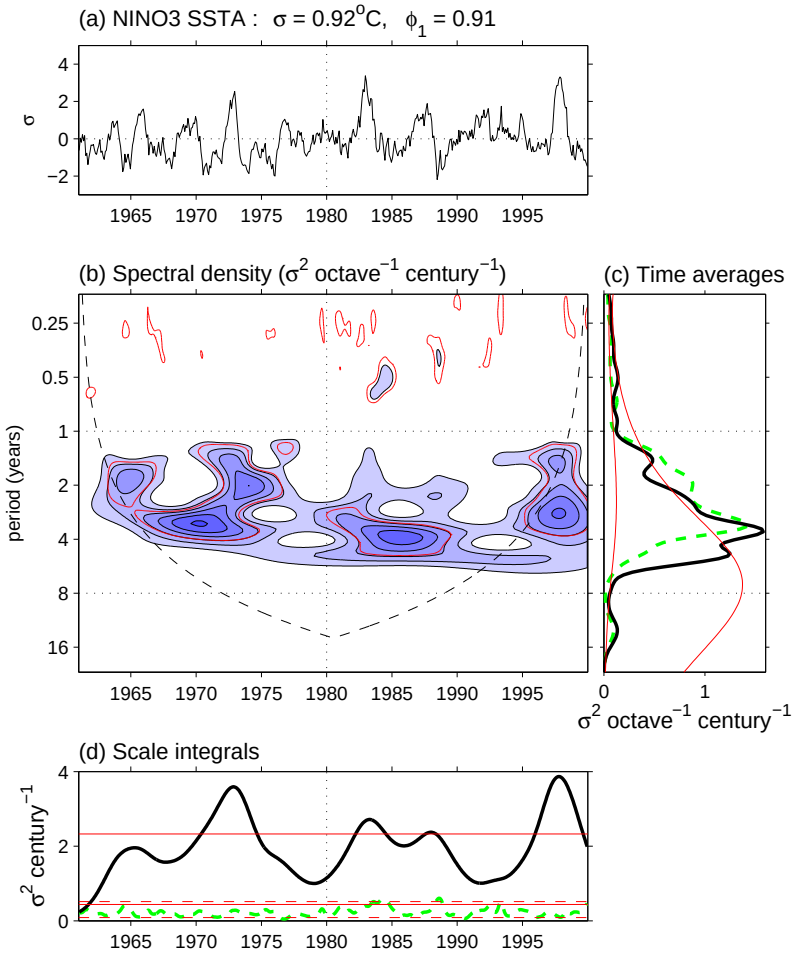

Figure 2.11: As in Fig. 2.9 but for SST anomalies averaged over the NINO3 region (150°W–90°W, 5°S–5°N).

than the NINO4 zonal stress anomalies in either NCEP ($\phi_1 = 0.82$) or FSU ($\phi_1 = 0.72$). For both stress products, τ_x' is well correlated with SSTA (0.65 for FSU, 0.74 for NCEP), with westerlies during El Niño and easterlies during La Niña.

Strikingly, the differences between the FSU and NCEP anomalies are of the same order as the stress anomalies themselves. The correlation of FSU and NCEP with each other (0.80) is only slightly larger than their correlation with SSTA. The FSU stress anomalies are generally stronger, noisier, and have broader westerly peaks than NCEP. Compared to NCEP or SSTA, FSU exhibits weaker interannual variability during the 1960s and 1970s, and weaker El Niño anomalies in 1982–83 and 1997–98. The 1991–92 El Niño event, on the other hand, is stronger in FSU than in NCEP or SSTA, stronger even than the 1982–83 and 1997–98 events in FSU. The 1996 cold event also shows up more strongly in FSU than in either NCEP or SSTA.

Around 1976–77, an upward "climate shift" is apparent in all three timeseries. This shift has been noted in a variety of datasets (Nitta and Yamada, 1989; Graham, 1994; Trenberth and Hurrell, 1994; An and Wang, 2000). Note that in NCEP, part of this shift may be an artifact related to introduction of satellite data around this time (Santer et al., 1999). However, the presence of this shift in a variety of fields, and its concurrence with changes in North Pacific climate, suggest that it may well be real and possibly independent of ENSO (Latif et al., 1997; Wang and An, 2002).

2.5.2 Spectra

Panels (b) of Figs. 2.9–2.11 give an alternate view of the timeseries. Wavelet analysis has been used by several authors to reveal interdecadal changes in ENSO (Gu and Philander, 1995; Wang and Wang, 1996; Torrence and Compo, 1999; Torrence and Webster, 1998, 1999). As pointed out by Lau and Weng (1995), a wavelet diagram amounts to a musical score for a timeseries, with low notes (long periods) at the bottom and high notes (short periods) at the top.

ENSO is evident in these diagrams as a concentration of variance between 1 and 8 yr, which is nonuniform in frequency and time. The blobs of variance are not much wider than the cone of influence, suggesting that ENSO events occur in isolated groups of one or two, separated by periods of reduced activity. The spectral power near 2 yr waxes and wanes in roughly an 8 yr cycle, while the power at 4 yr strengthens every 15 yr or so. There is also a gradual increase in variance at periods longer than 4 yr.

Panels (c) of Figs. 2.9–2.11 show the time-averaged spectra for 1961–1979 and 1980–1999. There is generally more power at subannual time scales for τ_x' than for SSTA, especially at periods of 3 months or less where τ_x' shows significantly more power than red noise. Both τ_x' and SSTA show broad peaks in the interannual band (1–8 yr) which become stronger after 1980. The spectral peaks at 12–15 yr are stronger in τ_x' than in SSTA, but the significance of these peaks is dubious since they cannot clearly be distinguished from red noise.

The spectra reveal many differences among the timeseries. The NCEP spectrum is more stationary in time than FSU, and looks more similar to SSTA than does FSU. This is perhaps to be expected since the NCEP model incorporates SST forcing into the analysis. In the 0–6 month band, FSU has relatively more power than NCEP and shows more of

an increase in variance after 1980 than either NCEP or SSTA. In the 6–12 month band, FSU shows significantly *less* power than the red noise spectrum, while NCEP and SSTA cannot be clearly distinguished from red noise. In the interannual band, FSU shows a much stronger increase in variance between 1961–1979 and 1980–1999 than either NCEP or SSTA. In FSU this increase is largest at a period of around 2.5 yr, at the short-period end of the active band. In NCEP and SSTA, the spectral change is best described as a shift of the entire active band toward *longer* periods.

Panels (d) of Figs. 2.9–2.11 show the running variances in the 0–1 yr band and the 1–8 yr band. The interannual SSTA variance has gradually changed over the past four decades, with quiet periods during the early 1960s, late 1970s, and early 1990s, and active periods during the early 1970s, mid-1980s, and late 1990s. Most of these changes are mirrored in the τ_x' data, though neither stress product shows reduced interannual variance during the early 1990s, when the decrease in variance at 4 yr was compensated for by an increase at 1–2 yr. The very strong El Niño of 1997–1998 and its aftermath correspond to highly significant interannual variance peaks in all three datasets.

The NCEP τ_x' variance is more uniform in time than either FSU or SSTA; the FSU interannual variance in particular increases strongly toward the latter half of the record. FSU and NCEP also show different changes in the 0–1 yr band: FSU shows heightened activity from 1983–1993, while NCEP shows fairly uniform noise activity apart from three prominent and isolated spikes in 1974–1975, 1982–1983, and 1997–1998.

The spectral variations of SSTA appear to be more consistent NCEP than with FSU. Again, this is not surprising since the NCEP reanalysis explicitly includes SST as a model forcing. NCEP also has a more stationary spectrum than FSU, probably because the NCEP analysis scheme is more rigorously uniform in time.

2.5.3 Seasonality of the anomaly variance

The annual cycles of NINO4 τ_x' and NINO3 SSTA variance are shown in Fig. 2.12. The standard deviation scales, labeled at the top of each plot, once again confirm that the wind stress anomalies (especially FSU) have a larger subannual component than do the SST anomalies. Column (a) indicates that the full anomaly variance depends on the calendar month. The SSTA variance, for example, is four times stronger in December than in March. The τ_x' variance also tends to peak near the end of the calendar year, though FSU is not as strongly locked to the annual cycle as NCEP. Between 1961–1979 and 1980–1999, there is not much change in the cycle of SSTA variance apart from an overall strengthening of the variance. The wind stress products, however, show more substantial changes. Both indicate an increased annual cycle of anomaly variance which peaks slightly later in the year: in NCEP, the December peak narrows and shifts to November, while in FSU the broad August–February peak shifts to September–March.

Column (b) of Fig. 2.12 shows that the interannual variances of τ_x' and SSTA are clearly phase-locked to the annual cycle, with anomalies most variable in boreal autumn and least variable in boreal spring. Between 1961–1979 and 1980–1999, all three datasets show a strengthening of the mean variance and a shift of the cycle of variance so that it peaks one month later in the year. However, while SSTA shows a weakening of the cycle of interannual variance, NCEP shows little change, and FSU actually shows a strengthening.

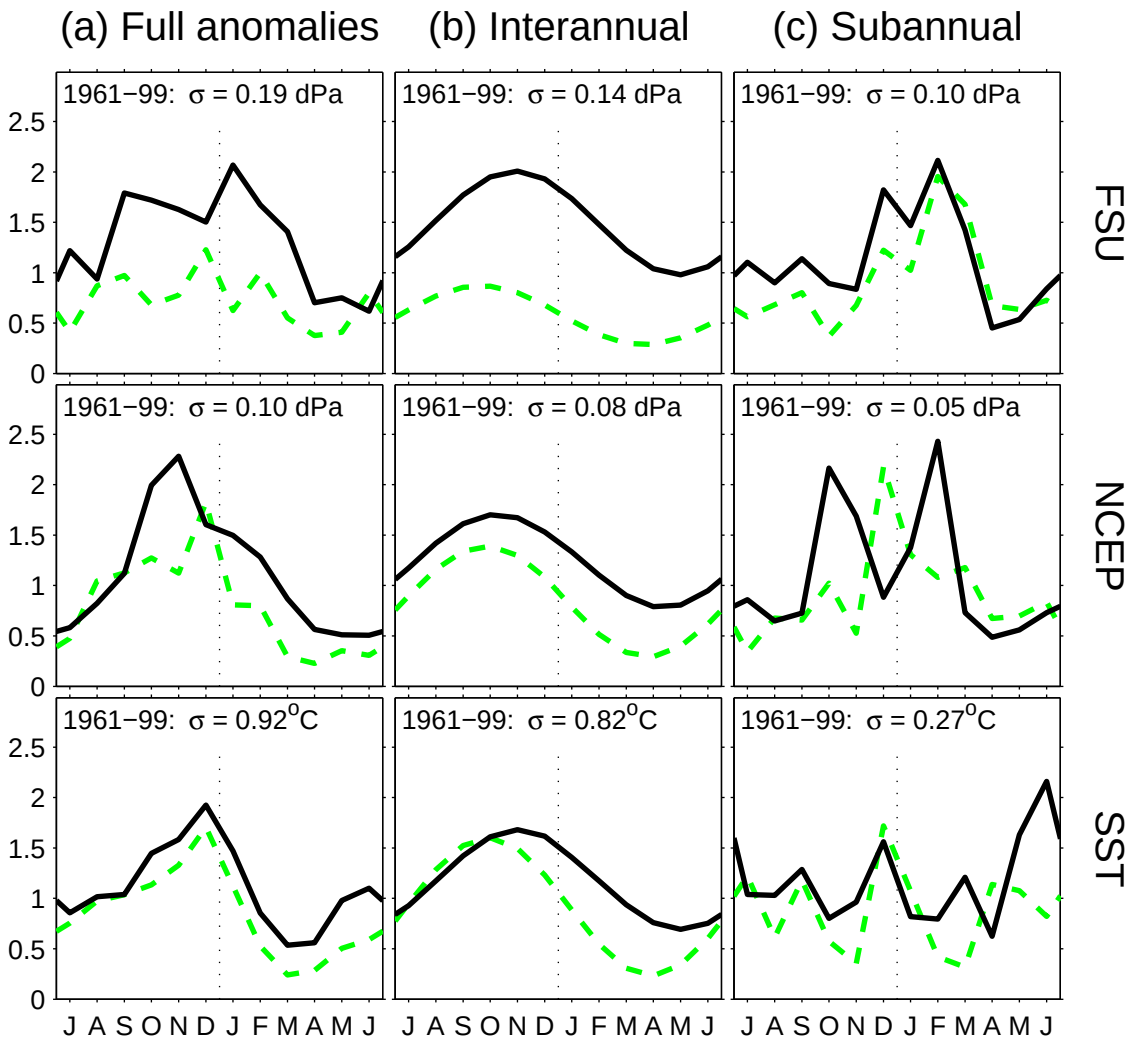

Figure 2.12: Monthly variance of the anomalies for FSU and NCEP τ_x' averaged over NINO4, and SSTA averaged over NINO3. The anomalies have been filtered to retain (a) all periods, (b) periods greater than one year, and (c) periods less than one year. The monthly variance, shown for 1961–1979 (dashed) and 1980–1999 (solid), is in units of σ^2 where σ is the standard deviation over the entire 1961–1999 period (labeled). The horizontal axis runs from July to June.

The cycles in the three datasets are all in phase during 1961–1979, but during 1980–1999 NCEP is shifted a few weeks earlier than FSU and SSTA.

Column (c) of Fig. 2.12 indicates that the seasonal cycle of subannual variance is more complex. Apart from a weak peak in December and a June peak during 1980–1999, the subannual NINO3 SSTA variance does not show much of a cycle. The subannual NINO4 τ_x' variance, however, shows a strong cycle with decreased variance in late boreal spring and summer and increased variance in boreal winter. Between 1961–1979 and 1980–1999, the subannual variance in FSU increased in every season except boreal spring, and the February peak in FSU broadened to include December and January. The December peak in NCEP, on the other hand, split into two separate peaks: one in October–November and the other in February.

Several conclusions can be drawn from Fig. 2.12. First, the calendar phasing of interannual anomalies is fairly robust, with little dependence on dataset and not much change between decades. Second, the phasing of the subannual "noise" is not as robust. It is usually assumed that the stress responds rapidly to SST (order of a few weeks or less), while SST responds slowly to the stress (∼2 months for subsurface Kelvin waves to cross the basin, plus time for upwelling to affect SST). If this is true, then the February peaks in subannual NINO4 τ_x' variance do not appear to be caused by subannual NINO3 SSTA. It is conceivable, though, that the February peaks in τ_x' produce the June peaks in SSTA activity. In addition, the December maxima in subannual τ_x', though curiously absent in the 1980–1999 NCEP data, could be related to the weak December peaks in subannual SSTA.

Considering the sharp features in Figs. 2.9a–2.10a, it is possible that nonlinearities contribute to the subannual maxima of NINO4 τ_x' variance. In particular, the subannual variance peaks in October–December occur at about the same time as the interannual variance peaks. Similarly, the subannual variance peaks during February–March occur at the time of year when the eastern Pacific is warmest, the ITCZ is closest to the equator, and equatorial convection is most active (Fig. 2.3). The idea that the climatology and ENSO may modulate the subannual variability is consistent with the conceptual framework of Meehl et al. (2001b).

2.5.4 Cross-correlations

Cross-correlations among the NINO4 τ_x' and NINO3 SSTA are shown schematically in Fig. 2.13. In this figure, hexagons symbolize the timeseries of Figs. 2.9a–2.11a, and connecting links indicate the correlations between the timeseries for 1961–1979 (inner links) and 1980–1999 (outer links). Clearly the interannual links are the strongest, with the correlations between the stress and SST nearly as strong as those between the stress products. The subannual correlations are much weaker: the subannual stress is completely independent of SST, and the subannual link between the stress analyses is rather tenuous. SSTAs are slightly better correlated with NCEP than with FSU, especially prior to 1980.

The changes in correlations between 1961–1979 and 1980–1999 are fairly small relative to the correlations themselves. There is almost no change in the links with SST, apart from a strengthening of the correlation between the full FSU and SST anomalies due to less negative subannual correlation. FSU and NCEP are generally in better agreement for

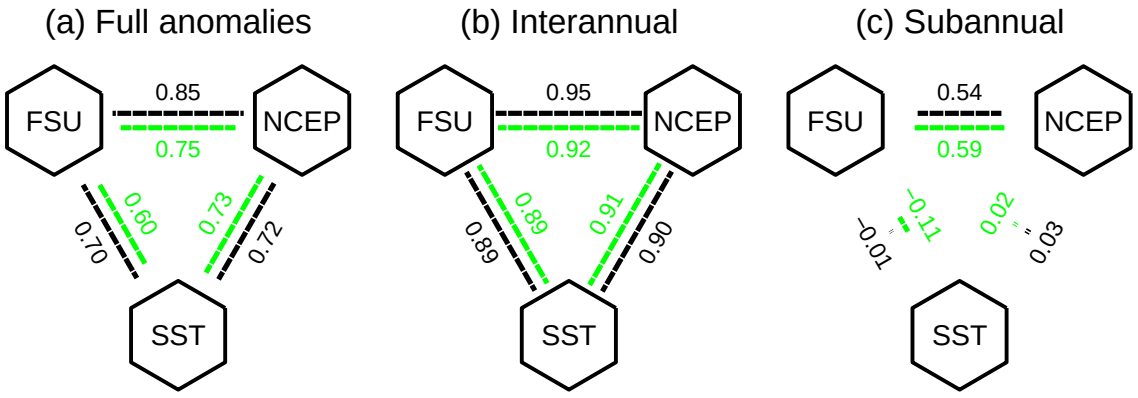

Figure 2.13: Correlations among FSU and NCEP NINO4 τ_x', and NINO3 SSTA, represented graphically by the length of the links between variables. Inner links are for 1961–1979, outer links are for 1980–1999. Correlations are shown for (a) the full anomalies, (b) anomalies filtered to retain only periods greater than 1 yr, and (c) anomalies filtered to retain only periods less than 1 yr.

the latter period, as evidenced by the increase in their correlation with each other (except at subannual time scales), and by their more similar correlations with SST.

2.5.5 Distributions

Probability densities

Probability densities of the interannual and subannual anomalies, estimated using a Gaussian kernel (Silverman, 1986), are shown in Fig. 2.14. On the basis of such plots one can make several qualitative statements. For the full anomalies, FSU appears more normally distributed than NCEP or SSTA, and for all three datasets, the subannual component looks more normally distributed than the interannual component. The interannual anomalies appear skewed to the right, more so for SSTA than for τ_x'. The subannual SST anomalies seem almost normally distributed. Between 1961–1979 and 1980–1999, some of the distributions appear to change, especially SSTA, which becomes more skewed to the right.

Red noise comparisons

One can use probability plots to quantify these statements. To assess the normality of a sample, for example, it is common to plot the sample quantiles against theoretical quantiles from a normal distribution. The correlation coefficient for this plot can then be tested for significant departures from unity, and if the departures are large enough then the hypothesis of normality can be rejected. This is the essence of the Shapiro-Wilks W-test for normality (D'Agostino and Stephens, 1986). In the present case, the monthly data are autocorrelated, so it is more appropriate to compare the sample quantiles with the quantiles of *autocorrelated* Gaussian red noise. Furthermore, it is easier to see the nature

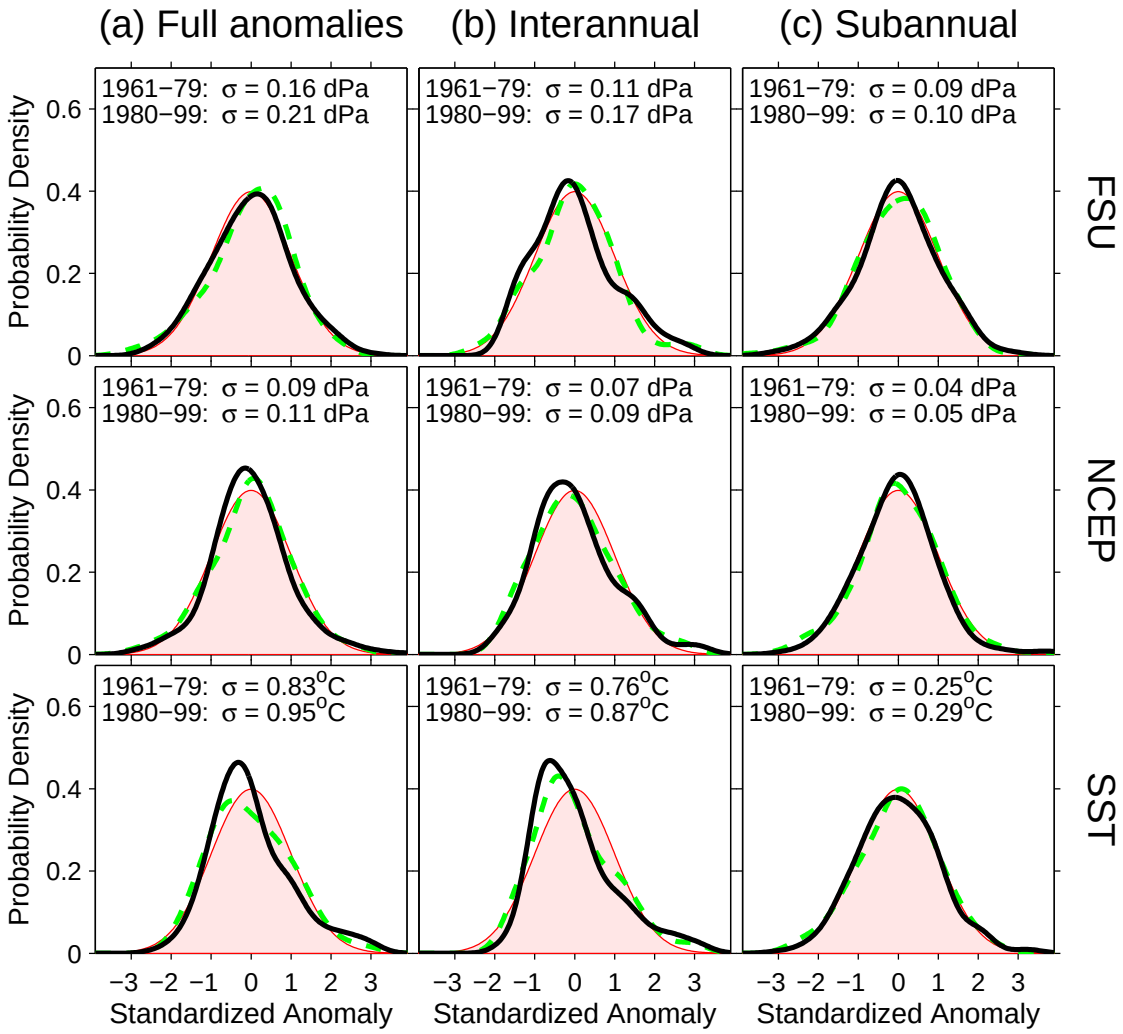

Figure 2.14: Distributions of standardized anomalies for FSU and NCEP τ_x' averaged over NINO4, and SSTA averaged over NINO3. The anomalies have been filtered to retain (a) all periods, (b) periods greater than one year, and (c) periods less than one year. The distributions, estimated using a Gaussian kernel, are shown for 1961–1979 (dashed) and 1980–1999 (solid). The normal distribution is shaded for reference.

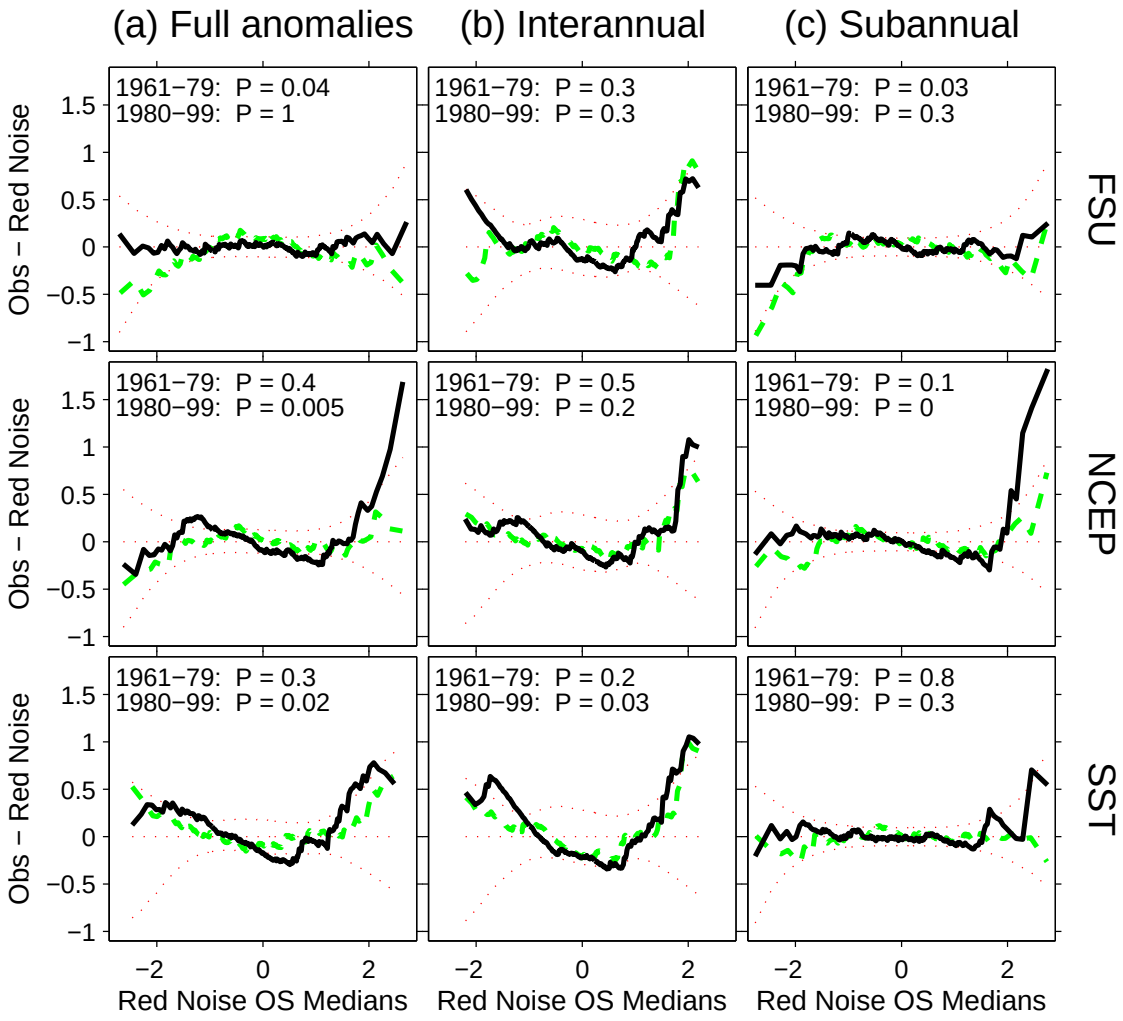

Figure 2.15: Normal probability plots of the data in Fig. 2.14, for 1961–1979 (dashed) and 1980–1999 (solid). The difference between the standardized ordered observations and the red noise order statistic medians is plotted against the latter. Under the hypothesis H_0 that the observations are red noise, one would expect this difference to be zero, apart from random fluctuations (curved dotted lines indicate the 95% confidence band from 10,000 red noise realizations). A test for normality is conducted using the correlation r between the ordered observations and the red noise order statistic medians. The probability that r could be as small as observed, under H_0, is estimated from the red noise realizations and given as P at the top of each plot.

of the non-normality if *differences* between the sample quantiles and red noise quantiles are plotted against the latter.

A set of such plots are shown in Fig. 2.15. If the data were simply Gaussian red noise, one would expect horizontal lines at zero. Concave-up curvature, on the other hand, indicates that both the smallest and the largest of the observations are larger than expected from red noise, i.e. the sample is skewed to the right. The curves may be considered consistent with red noise where they stay within the 95% confidence band (dotted lines). A test for the entire sample, similar to the W-test, is based on the correlation of the ordered data and the red noise quantiles. The probability that the correlation could be as small as observed, under the hypothesis that the observations are red noise, is given as P at the top of each plot.

With such a short data record, it is quite difficult to distinguish the observed distributions from red noise. There are simply not enough data: at interannual time scales, the 20-year timeseries essentially contain only 8 or so independent events. Thus the correlation test for red noise rejects only 6 of the 18 samples at the 0.05 level: full/subannual FSU for 1961–1979, full/subannual NCEP for 1980–1999, and full/interannual SSTA for 1980–1999.

Column (a) of Fig. 2.15 indicates the distribution of FSU anomalies is skewed to the left before 1980, but becomes indistinguishable from red noise after 1980. The NCEP distribution, on the other hand, is reasonably consistent with red noise before 1980 but becomes heavy-tailed (especially on the right) after 1980. The SSTA distribution is skewed to the right during both periods, more so after 1980.

Column (b) of Fig. 2.15 confirms that the interannual distributions are generally skewed to the right relative to red noise. However, the only sample that fails the correlation test is the post-1980 interannual SSTA. Thus the decadal changes in interannual τ_x' distributions, apparent in Fig. 2.14, are for the most part no larger than what one would expect from red noise. It would therefore be risky to interpret the apparent decadal changes in interannual distributions as anything more than random chance.

Column (c) of Fig. 2.15 shows that the subannual curves are reasonably flat over the bulk of each sample, suggesting consistency with red noise. Significant departures at extreme values, however, suggest a possible role for nonlinearity in FSU during 1961–1979 and in NCEP during 1980–1999.

Data cross-comparisons

Differenced quantile-quantile (DQQ) plots of NCEP versus FSU, and of each of these products versus SST, are shown in Fig. 2.16. Such plots offer a more direct comparison of the samples against each other. For identical samples the DQQ plot would be a flat line at zero. If the *leftmost* point in a DQQ plot of y versus x lies above the zero line, this indicates that the *smallest* value of y is larger than the *smallest* value of x. Similarly, if the *rightmost* point lies above zero, then the *largest* y is larger than the *largest* x. Finally, if the *center* point lies above zero, then the *median* of y is larger than the *median* of x.

The DQQ plots reveal some interesting relationships between the stress analyses. For the full anomalies, it is apparent that NCEP takes more extreme westerly values than FSU, especially after 1980. This is due to an increase in the subannual skewness of NCEP relative to FSU after 1980. Interannually, however, NCEP comes into better agreement

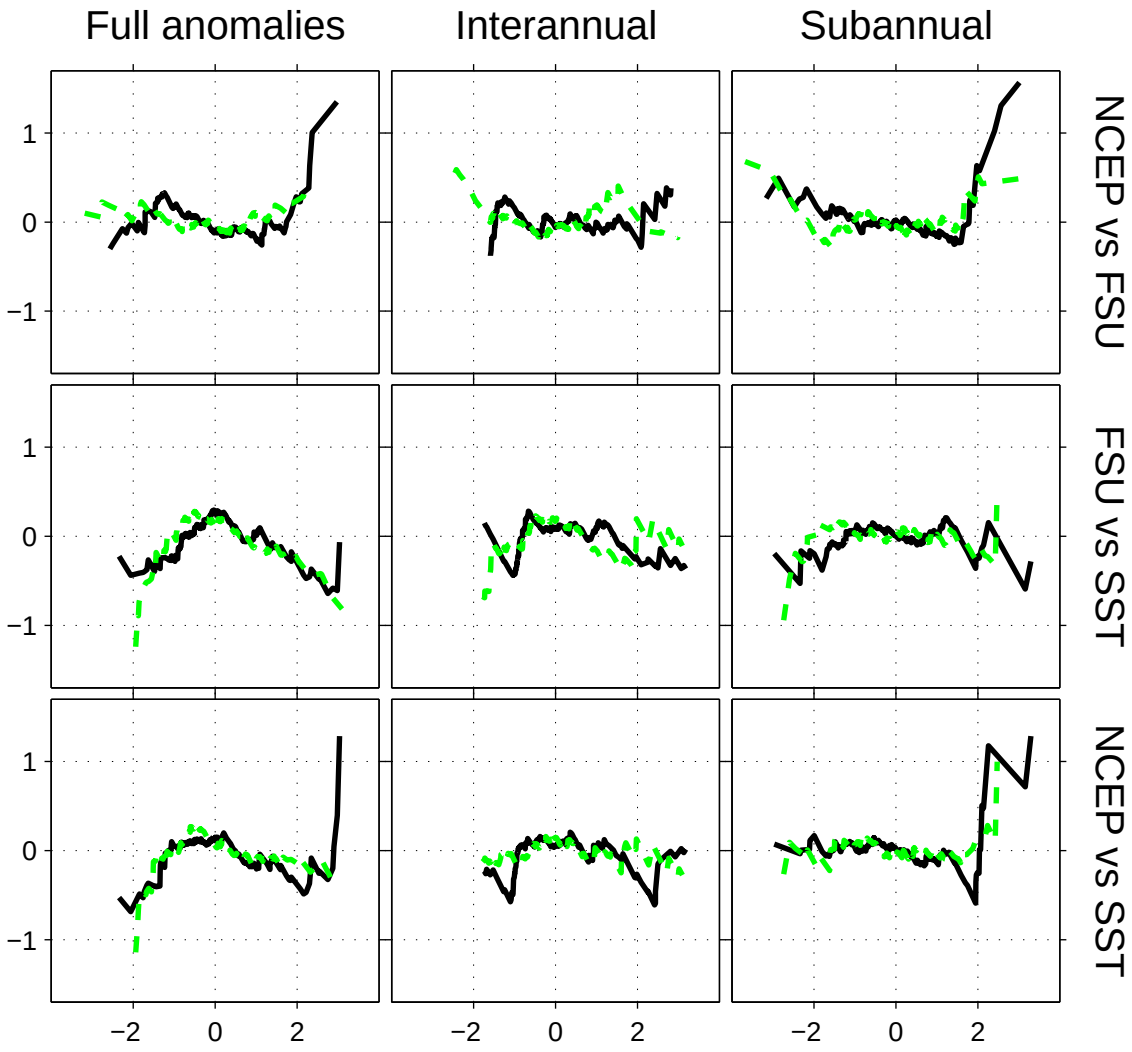

Figure 2.16: Differenced quantile-quantile plots of the data in Fig. 2.14, for 1961–1979 (dashed) and 1980–1999 (solid). Variables are indicated at the right edge of the figure; the difference between the standardized ordered observations of the first variable and those of the second are plotted against those of the second, for the full anomalies (left column), periods greater than one year (middle column), and periods less than one year (right column).

with FSU during the latter period.

The DQQ plots also reveal differences between the distributions of the wind stress anomalies and those of the SST anomalies. For the full anomalies, FSU is less skewed towards positive values than SST, although this difference decreases slightly after 1980. NCEP, however, shows an increasing tendency to take on more extreme positive values than SST, and a decreasing tendency to take on more extreme negative values than SST. The interannual distributions of τ_x' and SSTA are fairly similar. The subannual anomalies, however, indicate that FSU takes slightly more extreme *negative* values than SST, while NCEP takes much more extreme *positive* values than SST.

2.6 Conclusions

The tropical Pacific wind stress is a vital component of global climate but one which is difficult to estimate accurately. This study is the first to describe the full range of spatial and temporal variability of the observed wind stress and its consistency with observed SST in multiple datasets over a long time period. As such the results should be of great interest to researchers interested in tropical Pacific climate variability.

The NCEP stress climatology is distinguished from FSU by weaker equatorial easterlies, stronger off-equatorial cyclonic curl, weaker cross-equatorial southerlies in the east Pacific, stronger southerlies along the Peruvian coast, and weaker convergence zones with weaker annual variations. Changes in the mean state between 1961–1979 and 1980–1999 differ between the analyses, with FSU indicating an eastward shift and strengthening of the equatorial trade winds, but NCEP suggesting a westward shift and weakening of the trade winds. Modeling and data assimilation studies will be required to indicate which change is more consistent with the observed mean warming of tropical SST. Changes in the annual cycle of wind stress also differ between the analyses, but appear unrelated to changes in the annual cycle of SST.

In response to NINO3 SSTA, NCEP gives easterlies which peak farther east than in FSU. NCEP also exhibits a much weaker meridional stress response (owing to the weak convergence zones in that product) and lacks the cross-equatorial southerly anomalies evident in FSU. Between 1961–1979 and 1980–1999, FSU shows a strengthening and eastward spread of the zone of interannual τ_x' variability, while NCEP shows a weakening and westward spread of this variability. In this case the FSU change appears to be the more consistent with the observed increase in SST variability in the east Pacific. The changes in the wind stress response to NINO3 SSTA, if they are real, could be due to a slight change in the "meaning of NINO3 SSTA" over the past four decades (namely an eastward shift of the SST anomalies). Alternatively, the changes in wind stress response may be due to the observed change in climatological SST, which through nonlinearity would alter the strength and region of atmospheric heating induced by SST anomalies.

There is good temporal correlation of area-averaged western Pacific (NINO4) τ_x' between FSU and NCEP on interannual time scales. Small-scale stress anomalies, however, are not well correlated except for interannual anomalies in the western Pacific after 1980. Both interannual and subannual variability are stronger in FSU than NCEP, notably for τ_x' near the dateline and τ_y' near convergence zones. Although the anomalies are stronger and

noisier in FSU, NCEP shows more extreme westerly peaks in the NINO4 region during El Niño. Decadal changes in the distributions of subannual NINO4 τ_x' anomalies differ between FSU and NCEP, and large event-to-event differences between the analyses are evident.

The spectrum of NINO4 τ_x' in NCEP is more stationary in time than in FSU, and appears to be more consistent with NINO3 SSTA especially before 1980. Compared to FSU, NCEP shows a smaller fraction of the NINO4 τ_x' variability occurring at time scales of 3 months or less. Between 1961–1979 and 1980–1999, the interannual variability in FSU shifts toward shorter periods, while that in NCEP and SSTA shifts toward longer periods. The seasonal cycle of interannual variance becomes stronger in FSU, but does not much change in NCEP. The seasonal cycle of subannual variance and the decadal changes in this cycle are also quite different between the analyses.

Encouragingly, the wind stress analyses have come into better agreement since 1980, and many similarities are clear. At the equator between 1961–1979 and 1980–1999, both products show increased mean convergence in the far western Pacific, a weakening of the mean easterlies near the dateline, increased subannual and interannual variability in NINO4, and a stronger τ_x' response to SST anomalies. The following wind stress response to an eastern Pacific warming appears robust to dataset and time period: westerly anomalies peak in the west/central Pacific just south of the equator, while easterly anomalies appear off-equator and in the east; cyclonic stress curl anomalies in the north lie closer to the equatorial waveguide than in the south; and the anomalous stress is generally equatorward, except in the southeastern part of the basin. The interannual variance of NINO4 τ_x' peaks between October and November, the subannual variance between November and February. SST and stress anomalies are strongly correlated on interannual time scales, but uncorrelated on subannual time scales. Changes in the distribution of interannual NINO4 τ_x' between 1961–1979 and 1980–1999 are not significant.

Despite the better agreement since 1980, the FSU and NCEP stress analyses are very different. Changes in the analyses between 1961–1979 and 1980–1999 are generally smaller than the differences between the analyses, so the *true* changes in wind stress are very uncertain. Researchers should keep this uncertainty in mind when using the observed stresses to study climate variability, construct statistical atmosphere models, or drive ocean simulations.